Effect of ductile and frictional décollements on style of extension

Abbas Bahroudi*, Hemin A. Koyi, Christopher J. Talbot

Hans Ramberg Tectonic Laboratory, Institute of Earth Sciences, Uppsala University, Villavägen 16, SE-752 36 Uppsala, Sweden

Abstract

Scaled analogue models were used to study the effect of frictional and ductile detachments on thin-skinned extension. Models consisted of two halves; one half is the ductile and the other has a frictional detachment. Extension occurred above two different basal configurations: a stretchable rubber sheet and a folded, banded sheet intended to produce homogeneous and heterogeneous extension, respectively. Model parameters varied systematically and included the brittle/ductile thickness ratio, rheologies, and bulk strain. Structures in the two halves are compared in profiles and plan views. A series of graben developed above both halves of models extended above a banded sheet, although there were differences in style, propagation rate and width of the deformation zone between the two halves. Different rates of propagation of structures in the two halves led to the formation of an accommodation or transfer zone parallel to the extension direction. Most relay ramps and inflection of normal faults in this zone indicate differential extension between the two halves.

In contrast, in models extended above a stretchable rubber sheet, extensional structures such as horst and graben developed only above the ductile detachment. Model results indicate that heterogeneous mechanical stratigraphy and displacement rate have no effect on extensional structure above a rubber sheet. However, above 20% bulk extension, deformation becomes heterogeneous along multiple sets of conjugate faults oblique to the extension direction.

© 2003 Elsevier Science Ltd. All rights reserved.

Keywords: Extension; Analogue modelling; Ductile detachment; Frictional detachment

1. Introduction

The style of structures that develop in thin-skinned lateral shortening and thin-skinned lateral extension depends on the nature of the detachment. A detachment, décollement, abscherung, or sole fault may be defined as a "horizontal to low-angle basal stratum or fault which detaches an upper sequence involved in a deformation, from the underlying unit with less or no deformation" (e.g. Wernicke, 1981, 1985; Brun and Choukroune, 1983; Lister et al., 1987; Ramsay and Huber, 1987). Detachments or low angle fault surfaces can develop along weak boundaries or any significant sub-horizontal mechanical discontinuity. They may develop on any scale and at a level in the Earth's crust, but commonly detach a weak sedimentary sequence from its underlying crystalline basement, which either controls deformation of the cover units or remains a rigid and stable basal unit (Mandl, 1988). On the basis of their mechanical behaviour in the uppermost part of the crust, two

types of detachments are distinguished: frictional and ductile detachments. Sedimentary rocks, such evaporites, particularly rock salt or overpressured shale, behave as ductile detachments (e.g. Chapple, 1978; Davis and Engelder, 1985, 1987; Koyi, 1988; Gaullier et al., 1993; Letouzey et al., 1995). Bedding boundaries or the contact between a sedimentary cover and its basement act as a frictional detachment. There have been many model studies of extension on ductile detachment (Brun et al., 1985; Vendeville, 1987; Vendeville et al., 1987; Cobbold et al., 1989; Vendeville and Jackson, 1992; Benes and Davy, 1996; Withjack and Callaway, 2000). However, few models have been reported of extension over frictional detachments. This is probably because it is technically more difficult to extend models above such décollements. It has been common to model frictional detachments by extending a thin plastic or rubber membrane at the base and report the resulting asymmetric and symmetric thin-skinned extension structures (Cloos, 1955; McClay and Ellis, 1987a; Vendeville et al., 1987; Mandl, 1988; McClay, 1990, 1996; Ishikawa and Otsuki, 1995; Keep and McClay, 1997; Kerr and White, 1996).

* Corresponding author.
  E-mail address: abbas.bahroudi@geo.uu.se (A. Bahroudi).

In this paper, we use scaled sandbox models to investigate and compare the style of thin-skinned extension above frictional and ductile detachments in the upper crust. Here, we also use a rubber sheet to extend homogeneously some of our models.

2. Experimental method

This study documents 11 models subjected to thin-skinned extension in order to simulate deformation in the upper crust. Many studies of extended regions show that active structures in the crystalline basement, or irregularities in its top surface, control the deformation accommdated in the cover (e.g. Colletta et al., 1988; Gaullier et al., 1993; Kusznir et al., 1995; Schlische, 1995). Therefore, we have also investigated the effect of the reactivation of basement faults and localisation of normal faulting in the cover.

The base of all models was planar and horizontal. Each model was divided into two equal halves, either parallel to the extension direction or, in one model, oblique to it (Fig. 1). One half had a layer of loose sand resting on a ductile detachment (DD) consisting of a layer of silicon
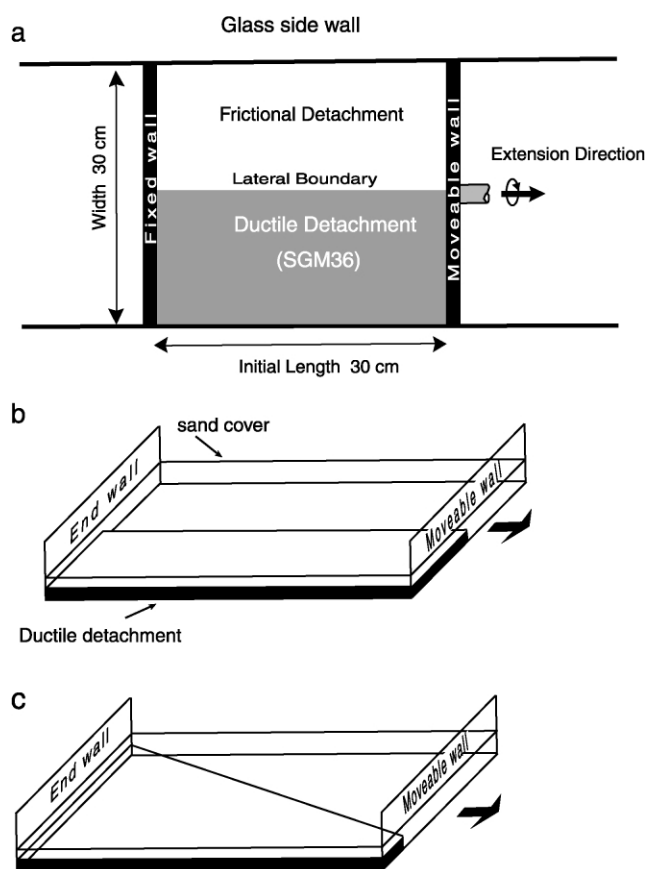

Fig. 1. Schematic illustration of configuration of the extensional models: (a) plan view of initial state of the models in the deformation rig, (b) schematic illustration of configuration of the models except models 5 and 8, and (c) schematic illustration of the configuration of model 5.

(SGM-36) and the other half had either a frictional detachment (FD) with a layer of loose sand or a low-friction detachment consisting of glass beads (Table 1), resting directly on a rigid substrate (Fig. 1a).

The Newtonian viscous material PDMS (SGM-36) is a suitable material for simulating the ductile behaviour of evaporites or shale, whereas loose sand is appropriate for simulating the frictional behaviour of non-evaporitic sediments (e.g. Werijermars et al., 1993).

The sand layers were constructed to the desired thickness by sieving alternating layers of rounded grains of sand, about ≥ 35 μm in size (Table 2). The bulk density of the loose sand is $\rho_m = 1700$ kg m^{-3} with a cohesive strength $C_m = 140$ Pa (Cotton and Koyi, 2000). The silicon (SGM-36) manufactured by Dow Corning Ltd, has an effective viscosity of $\eta_m = 5 \times 10^4$ Pa at room temperature (~ 20 °C); its density is $\rho_m = 987$ kg m^{-3} (see Table 2).

Two different basal configurations were used to extend in the models. A folded banded sheet resulting in stepwise extension was used to simulate small displacements along basement faults; and a rubber sheet was used to simulate homogeneous extension. These two basal sheets were attached to the end walls, one of which was moved away from the other, simultaneously pulling the attached sheet (Fig. 2).

The folded banded sheet was made of alternating sequential strips of thin (2 cm wide), rigid plastic attached to each other by a soft plastic sheet, which was initially folded beneath one of the rigid plastic strips. (Fig. 2b). These strips were placed next to one another to form an expandable substrate on which the sand layers were built.

The stretchable rubber sheet was similar to those used by other workers to simulate thin-skinned homogeneous extension (Fig. 2a; e.g. Cloos, 1955; McClay and Ellis, 1987a,b; McClay, 1990; Ishikawa and Otsuki, 1995). The rubber sheet was 34 cm wide, 30 cm long and 0.1 cm thick. The starting dimension of the models was 30×30 cm (Fig. 1a). Models were built in a deformation rig that was placed on an aluminium-topped table representing a rigid basement (Fig. 3). Uniaxial extension was applied by moving one wall, which stretched the rubber sheet or banded sheet at the base of the model. The constant displacement rate of the movable wall, $\nu = 3.2 \times 10^{-4}$ cm/s, was controlled by a motor-driven worm screw.

A square grid (1.2×1.2 cm) of negligible thickness was masked on the top surface of each individual model. At regular time intervals, the surface of the model was photographed to record the surficial structures during extension. Measurements were also made in situ. Following Koyi et al. (2000), displacement along normal faults was monitored by marker points placed on the surface of the footwall and hanging wall of each new fault as it developed. The distance between each pair of marker points was measured throughout model deformation. After the desired amount of bulk extension, models were covered by loose sand and impregnated by water. This process increases the

Table 1
Model specifications

Model	Thickness of ductile layer (cm)	Thickness of sand layer (cm)	Brittle/ductile thickness ratio	Basement	% Bulk extension	Remarks
MDL-1	1.2	2.4	2	Strip sheet	17	
MDL-2	1.2	2.4	2	Stretchable sheet	18	
MDL-3	0.8	2.4	3	Stretchable sheet	20	
MDL-4	0.8	2.4	3	Stretchable sheet	19.5	Localized extension
MDL-5	1.2	2.4	2	Stretchable sheet	21	Oblique pattern
MDL-6	0.4	2.4	6	Stretchable sheet	20.5	
MDL-7	0.6	2.4	4	Strip sheet	18	
MDL-8	0.6	2.4	4	Stretchable sheet	20	
MDL-9	0.0	3		Stretchable sheet	46	Fast extension
MDL-10	0.6	1.2	2	Stretchable sheet	20	
MDL-11	0.8	2.4	3	Stretchable sheet	20	Glass beads

cohesive strength of sand and allows the cutting of vertical sections for photography.

3. Model scaling

To simulate any natural process by analogue modelling, it is necessary to scale the model using the principles of physical similarity, e.g. Hubbert (1937) and Ramberg (1967, 1981). A model should be scaled geometrically, kinematically and dynamically to its prototype. In our models, the length ratio is 10^{-4} to 10^{-5} implying that 1 cm in the model simulates 1–10 km in nature.

The models presented here are not intended to represent the structural evolution of any particular region. Therefore, kinematic similarity could be approached qualitatively by proposing a realistic geological situation. Thus, we consider a region containing, for instance, a sedimentary cover sequence deposited on the flat-top of a rigid basement. The region can be divided into two halves. In one half, a ductile detachment layer of evaporites, for example, decouples the sedimentary cover sequence from the basement. In the other half, the sediments rest directly on the basement.

The Coulomb–Mohr criterion, which predicts the rheological behaviour of brittle material, can be used to calculate ratios of the dynamic similarity between models and nature. The Coulomb–Mohr criterion contains some intrinsic material properties, such as cohesive shear strength (C_o) and coefficient of internal frictional (μ), which should be equal in 1 g model and nature in order to achieve dynamic similarity:

$$\tau = C_o + \sigma\mu \qquad (1)$$

Here τ and σ are shear and normal stresses on the fault plane and $\mu = \tan\phi$, with ϕ being the angle of internal frictional of faulted material. The angle of internal frictional of brittle upper crust and sediments range between $\phi_n = 31°$ and $40°$, which gives a coefficient of internal frictional ranging between 0.6 and 0.84, with the cohesive strength C_n of about 50 MPa (Byerlee, 1978; Brace and Kohlstedt, 1980; Cobbold et al., 1989; Gaullier et al., 1993; Koyi et al., 1993; Werijermars et al., 1993; Benes and Davy, 1996). Loose sand with the same internal frictional angle, $\phi_m = 36°$ giving a coefficient of internal frictional $\mu_m = 0.73$ (Krantz, 1991; Cotton and Koyi, 2000) and negligible cohesive strength, is a nearly prefect Coulomb–Mohr material for simulating the brittle behaviour of typical sedimentary covers. To scale the model dynamically, the non-dimensional shear strength, τ/σ, in the model and nature should be equal, i.e $\tau/\sigma \sim 1$ (Mulugeta, 1988; Childs et al., 1995; Cotton and Koyi, 2000). Dividing Eq. (1) by σ,

Table 2
Scaling parameters between model and nature

| Parameter	Model	Nature	Model/nature ratio
Length (m)	0.01	$1 \times 10^{3 \text{ to } 4}$	$1 \times 10^{-4 \text{ to } -5}$
Density of brittle layer (kg m^{-3})	1700	2550–2700	0.59
Density of ductile layer (kg m^{-3})	987	2200	0.45
Density contrast (kg m^{-3})	500–700	350–500	1.46
Viscosity of ductile layer (Pa s)	5×10^4	$1.7 \times 10^{18 \text{ to } 19}$	$2.9 \times 10^{-14 \text{ to } -15}$
Angle of internal friction	36°	31–40°	~ 1
Coefficient of internal friction of brittle layer	0.6	0.6–0.84	0.7–1
Cohesion of brittle layer (Pa)	140	5×10^7	3.5×10^{-6}
Gravity acceleration (m s^{-2})	9.81	9.81	1
Time (s)	3600	315×10^5	
Rate of displacement (cm s^{-1})	$3.2 \times 10^{-3 \text{ to } -4}$	$\sim 3.17 \times 10^{-8}$	$\sim 1 \times 10^{4 \text{ to } 5}$
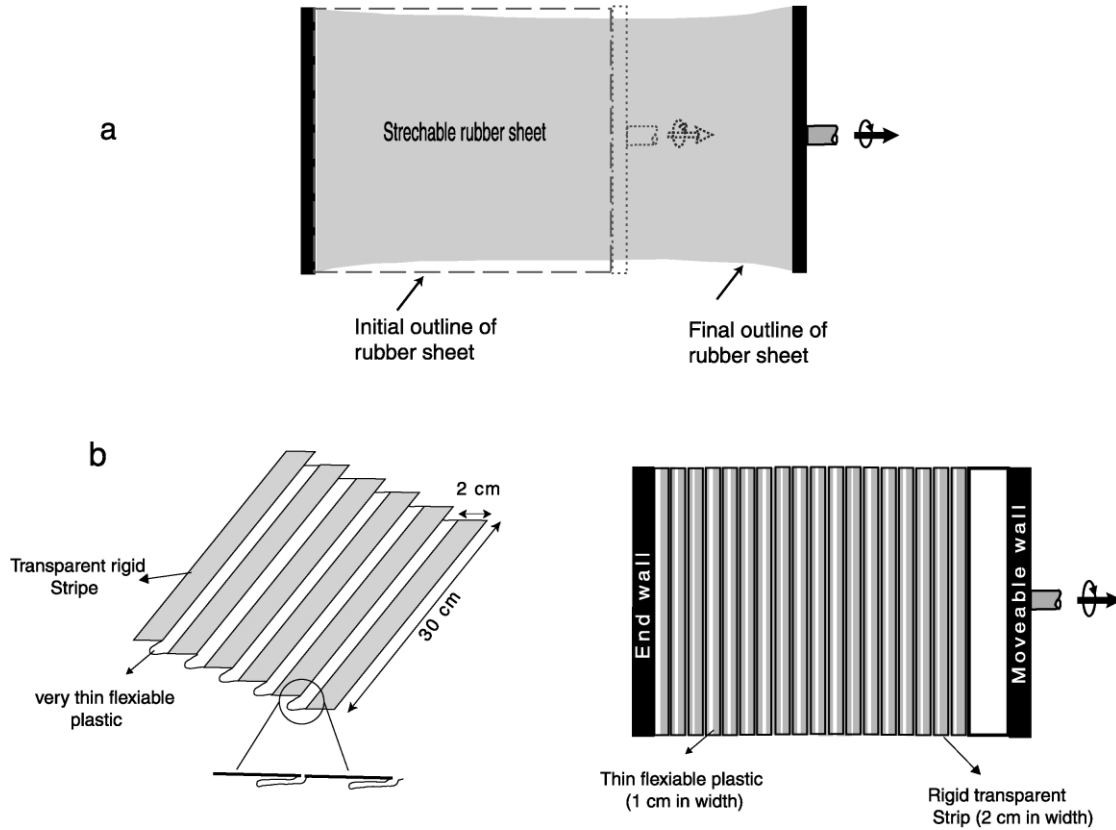
Fig. 2. Basal configuration of the extended models: (a) configuration of the stretchable rubber sheet at the base of sand pack, and (b) configuration of the linked, plastic strip basement.

gives:

$$\tau/\sigma = \mu\sigma/\sigma + C_o/\sigma \Rightarrow \tau/\sigma = \mu + C_o/\sigma$$

A similar τ/σ ratio for the model (m) and nature (n) is:

$$(\mu + C_o/\sigma)_m = (\mu + C_o/\sigma)_n \tag{2}$$

Because μ_m and μ_n (Table 2) have approximately similar values, they can now be neglected in Eq. (2), which will be rewritten as:

$$(C_o/\sigma)_m = (C_o/\sigma)_n \tag{3}$$

Since the normal stress σ can be defined as:

$$\sigma = \rho g l \tag{4}$$

where ρ is density, g is the gravitational acceleration and l is the length, Eq. (3) can be rewritten as:

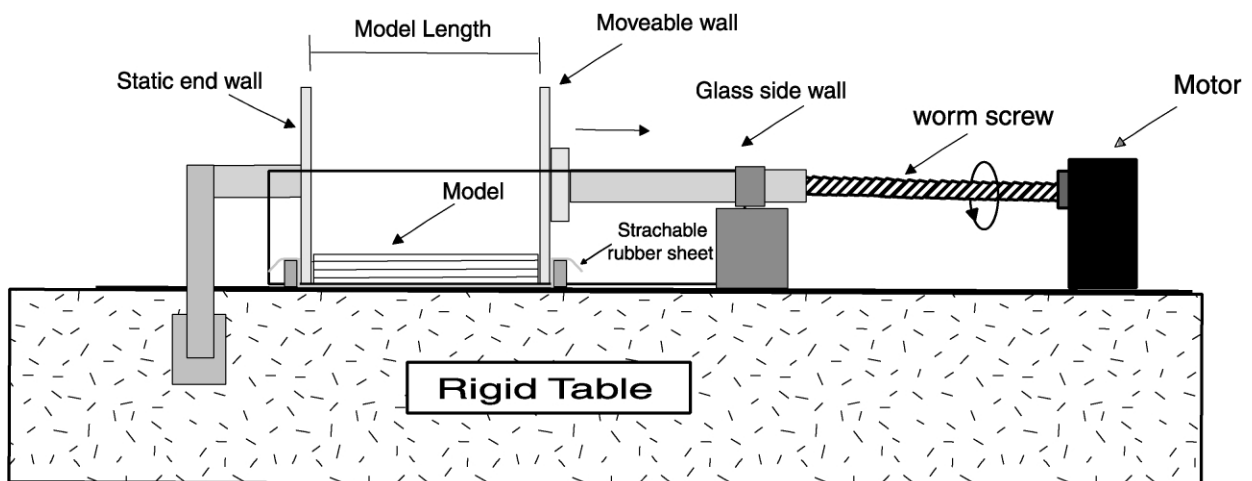$$(C_o/\rho g l)_m = (C_o/\rho g l)_n \tag{5}$$

Fig. 3. Schematic profile of the uniaxial extension rig used to extend the models.

Substituting the values given in Table 2 into Eq. (5), the non-dimensional shear strength values will be 1.8×10^{-1} and 7.1×10^{-1} for nature and model, respectively. These are within the same order of magnitude, suggesting approximate dynamic similarity between the models and nature.

4. Model kinematics and result

All models were extended at a constant rate of 3.2×10^{-4} cm s^{-1} except for model 9 where the rate was faster (about 5×10^{-3} cm s^{-1}). Below, we describe the two main groups of models: a group extended in small increments above a banded sheet and a second group extended smoothly above a rubber sheet.

4.1. Step-wise extension

These experiments aimed to simulate reactivation of basement faults and the associated nucleation of faults in the sand layer within restricted zones where and when the rigid strips separated (Fig. 2b). For this series, two models (1 and 7) with different brittle/ductile thickness ratios, were extended above a banded sheet (Table 1). In spite of some similarities, these models looked very different in profiles and plan views in the FD and the DD halves after extension (Figs. 4 and 5).

4.1.1. Comparison of plan views

The final plan view of models 1 and 7 display a series of horst and graben (Figs. 4c and 5b). The deformation zone above the DD is generally wider than that above the FD. The faults above the DD halves propagated faster and further than those in the FD halves. Faulting above the ductile detachment developed after smaller bulk extension, e.g. 3%, compared with faulting that began after >5% extension above a FD.

In plan view, most normal faults are bent at the boundary between the DD and FD halves in models 1 and 7 (Figs. 4a and c and 5b). This inflection reflects the different styles of extension between the DD and the FD halves. Fault inflections are profound in model 1 where the brittle/ductile thickness ratio is lower than in model 7 (see Table 1). By reducing the thickness of the basal ductile layer, the effect of viscous drag along the base of the sand layer increased, which restricted propagation of the deformation front.

4.1.2. Comparison of recovered profiles

Recovered profiles through the FD half of models 1 and 7 are shown in Figs. 4b and 5a, respectively. These profiles show that deformation was accommodated in a main rift zone by horst and graben. Some of the normal faults defining the grabens not only intersect but also displace each other indicating that they were active sequentially. In model 7, counter regional (CR) normal faults dip in the direction opposite to the extension direction, and appear to intersect

regional (R) faults, which dip in the same direction as the extension direction (Figs. 4b and 5a). All faults are normal and dip 55–60° on average regardless of dip direction. The horst/graben structures developed in model 7 were more regular than in model 1 where the spacing of regional and non-regional faults are similar (Fig. 5a). Although most of the normal faults are planar, some in model 7 are subplanar (see Figs. 4c and 5b).

Structures developed above the DD half of models 1 and 7 differ from those developed above the FD half (Figs. 4d and 5c). Above the ductile detachment, extension in the sand layer covered a wider area that consists of horsts and grabens that developed sequentially. Normal faults were subplanar with an average dip of 55° in both direction but sole out into the ductile detachment without intersecting each other.

Comparison of the final extended length of models with their initial lengths above the FD show that most of the extension occurs along the normal faults, where it results in penetrative strains in narrow zones in which the packing of sand grains changed.

Comparison of profiles recovered from the DD and the FD halves show that:

1. Extension is accommodated in a wider zone above the DD.
2. Normal faults are steeper $\cong 60°$ above the FD.
3. Normal faults do not intersect above the DD.
4. Block-rotation is more common above the DD.
5. Normal faults are clearly more numerous above the FD.
6. Penetrative strain occurs above the DD.

4.2. Homogenous extension

Another series of models, including 2–6 and 8–11 was extended over a stretchable rubber sheet (see Fig. 2a). In four of these models (2, 3, 6, and 10) the brittle/ductile thickness ratio was increased from two to six in the DD half (see Table 1), to study the effect of this ratio on extension of a sand layer. Model 5 and 8 were prepared to study the effects of the distribution of ductile detachment and heterogeneous mechanical properties in the cover. In order to study the effect of homogeneous extension (over 20% of bulk extension) on sand layers (model 9), which had no ductile layer, was extended directly above a rubber sheet. In this model, the rate and amount of extension were exceptionally high compared with the other models (see Table 1). Model 11 was prepared to study the effect of a low frictional detachment (LFD) using an 8-mm-thick layer of fine grain glass beads between the rubber sheet and the sand layer.

4.2.1. Comparison of plan views

Development of normal faults in models 2, 3, 6, 8, 10 and 11 are almost all restricted to the DD halves (Figs. 6a, 7b and 8a). Apart from a few faults generated close to the end
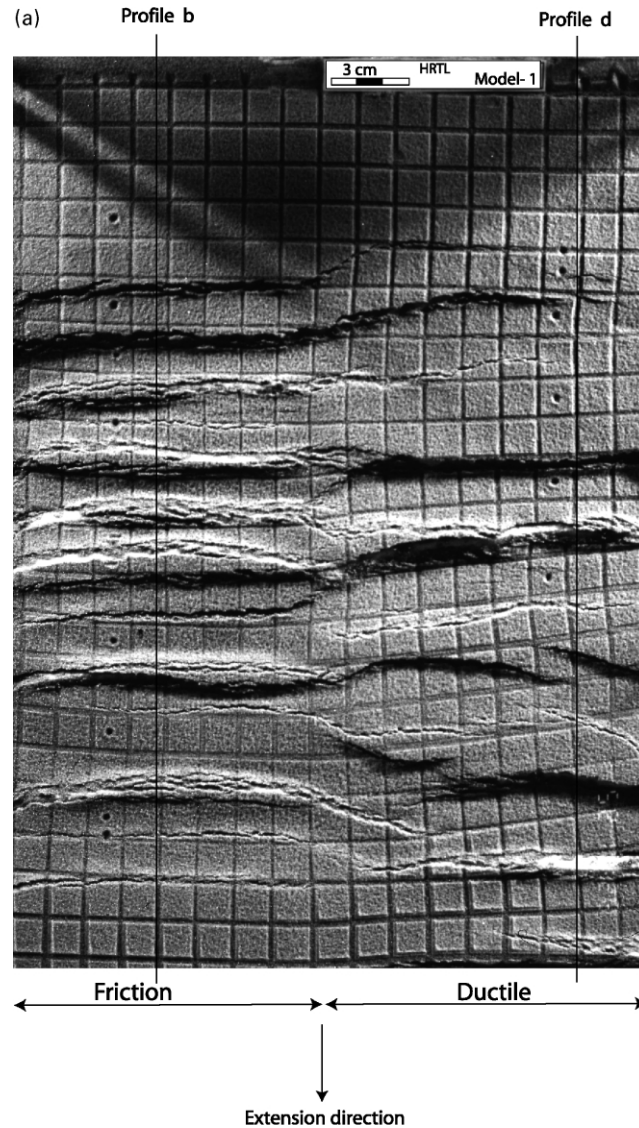
Fig. 4. Photograph and line drawings of profiles and plan view of model 1 after a bulk extension of 16.5%. (a) Top-view photograph, (b) the FD half shows closely spaced horst-graben structures above active stripes, dark and small rectangulars, (c) model plan view showing development above the FD and DD halves, and (d) the DD half with wider horst and graben in a longer deformation zone.

walls, no faults formed in the sand layer above the FD halves. Instead, the marker grid extended homogeneously and uniformly above the FD. Measurements of square markers on the surface of the deformed models above the DD half and the FD half indicate some differences in strain distribution. Square markers above the ductile detachment show some penetrative strain usually between zero and 10%. Instead, markers were extended homogeneously and uniformly above the FD half.

The boundary between the DD and the FD halves of the models is mainly indicated by development of small fractures and fissures where the normal faults that developed above the DD half die out into the FD half, particularly in models 2 and 3 (Figs. 6a and 7b).

By contrast with other models (e.g. models 1–4, 6–8 and 10) the boundary between the DD and FD halves in model 5

was oblique to the extension direction with a low brittle/ductile ratio (~2) (see Table 1 and Fig. 1c). The top view of model 5 after a bulk 21% extension (Fig. 9b) shows that the pattern of normal faults in the cover relates to the configuration of the ductile substrate (see also Gaullier et al., 1993; Fig. 9a and b). The variation of lateral propagation of structures formed in the overlying sand layer was controlled by distribution of the DD. Normal faults were restricted to the DD half and only a few extended as much as 2 cm across the junction (Fig. 9).

Model 9 was the only model in which the DD half was absent and the model was extended at a faster rate than the others (see Table 2). No obvious normal fault had developed in this model by 20% bulk extension. At higher bulk extension (>20%) a pattern of oblique faults formed that gradually amplified as the bulk extension increased to 46%

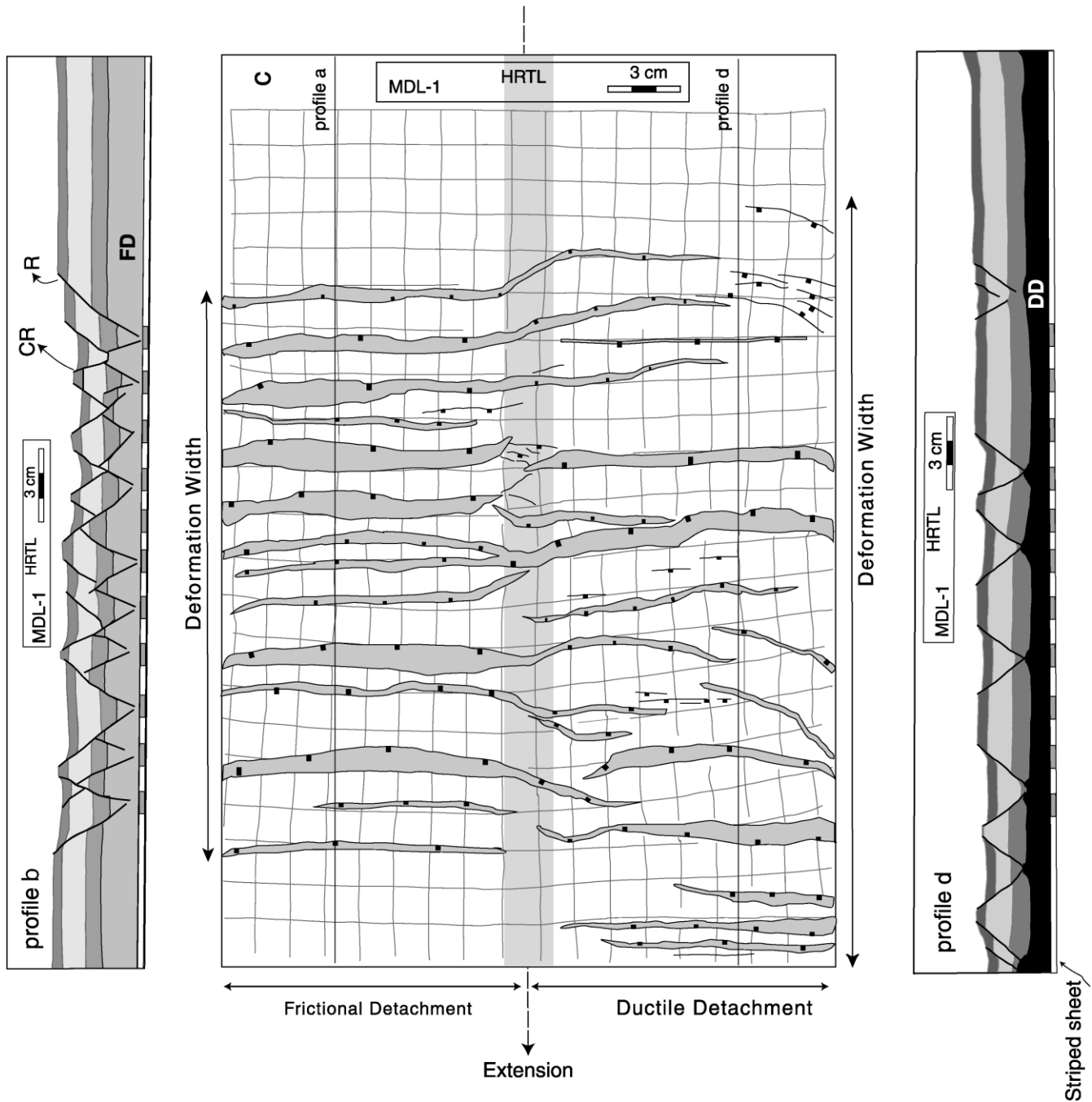Fig. 4 (*continued*)

(Figs. 10 and 11). Deformation of the initially square reference grid indicates that the fault pattern consists mainly of two sets of conjugate faults, which show both dip and strike-slip movements (Fig. 10a and b). All these faults developed early (~25% extension) and almost synchronously, and remained active throughout most of the deformation. Each of the two conjugate sets of faults is restricted to particular parts of the model and they do not appear to intersect each other. The left-lateral faults in the central part of the model in top view are longer and further

apart (1.3 cm) than shorter and closer faults (0.97 cm) in marginal areas (Fig. 10). The majority of these faults dipped toward the extension direction (Fig. 11).

In model 11, where glass beads were used to simulate a low frictional detachment (LFD), some normal faults developed above the DD half as expected from other models. These faults propagated slightly into the LFD half across the mutual boundary. A plan view of model 11 shows some faults with very small displacements plus some vertical dilation fissures formed in the sand layer particularly close
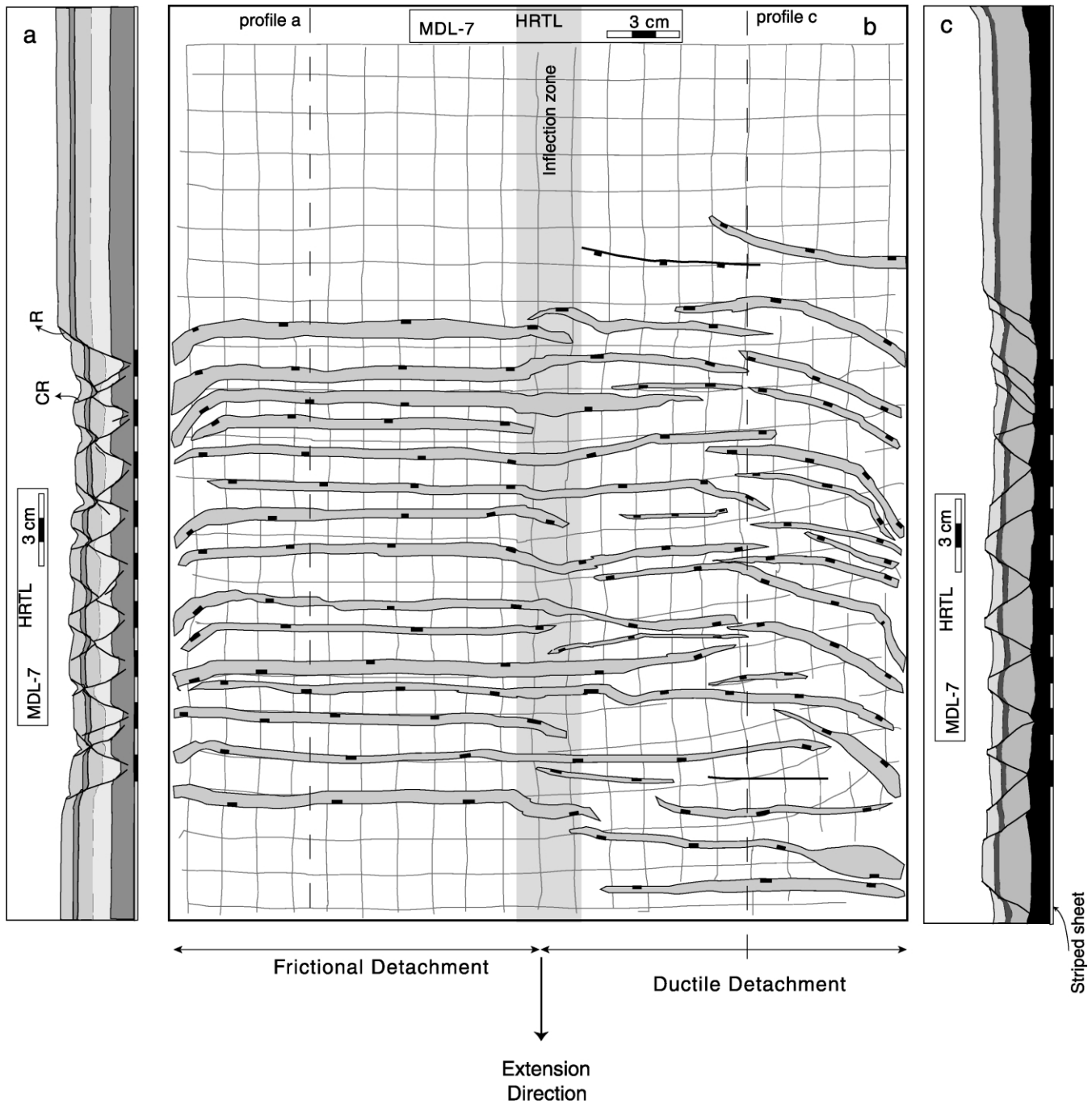
Fig. 5. Line drawing of profiles ((a) and (c)) and plan view (b) model 7 after it was extended by 18% above the banded basal sheet: (a) the FD half showing horst-graben structures above active stripes, (b) plan view showing development of normal faults above the halves, and (c) the DD half showing wider deformation zone in comparison to the DD half.

to the boundary after 20% of bulk extension. However, these faults appear to die out by the centre line of the LFD half.

4.2.2. Comparison of profiles

In the DD halves of models 2, 3 and 6, extension was accommodated mainly by well-defined normal faults, which began to form near the moving wall and developed sequentially toward the fixed wall (Figs. 6b, 7c and 8b). In

model 2, where the ductile substrate was thick (1.2 cm), a reactive diapiric structure rose where the sand layer was thinned after a bulk extension of ~20% (see Fig. 6b; fig. 5 in Vendeville and Jackson, 1992). Conjugate pairs of (R and CR) normal faults formed horsts and grabens. The faults increased in number from model 2 to model 6 and all soled into the ductile detachment. However, comparison of profiles of the DD halves of models 2–6 (Figs. 6b, 7c and 8b) shows that the normal faults tended to intersect each
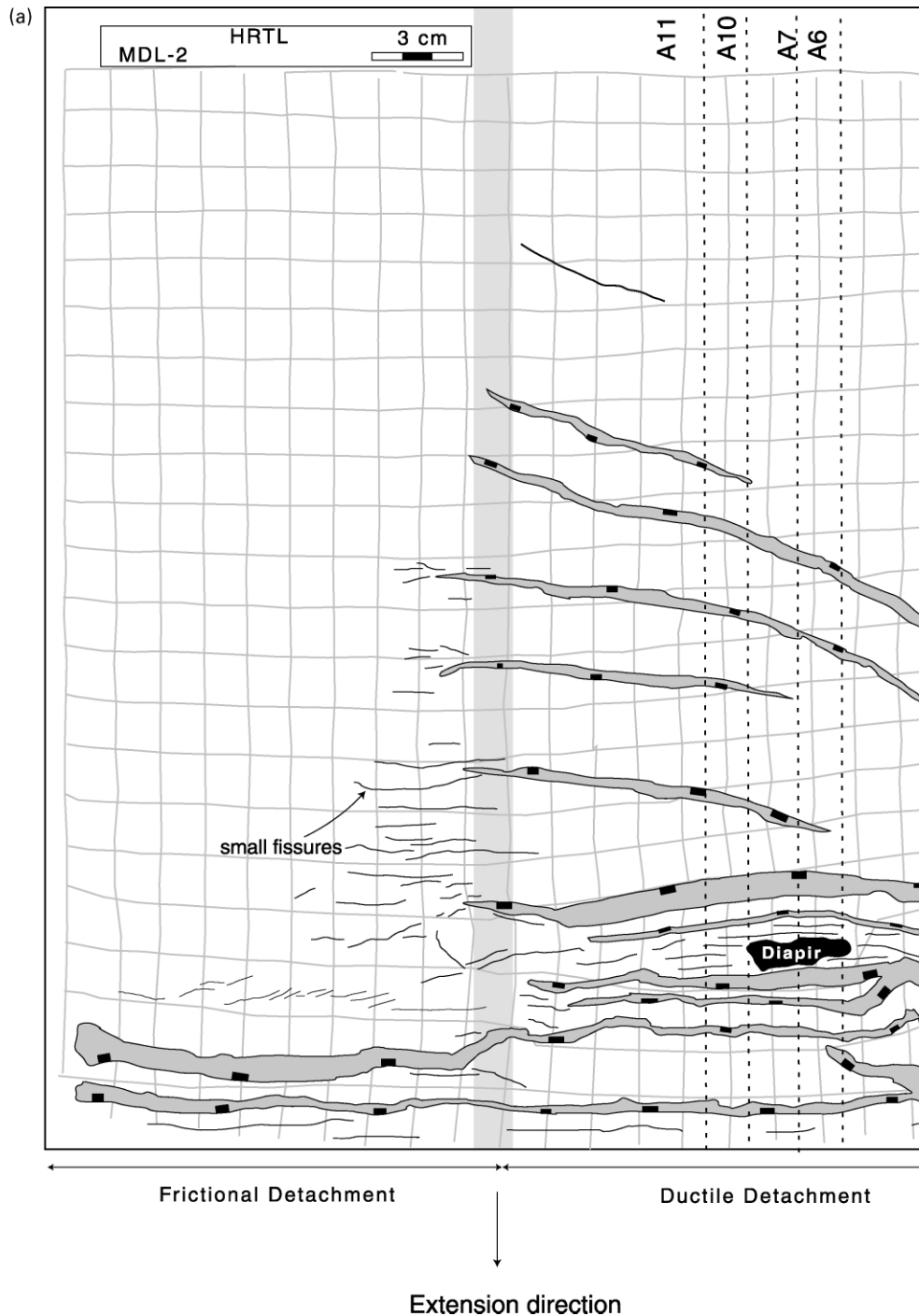
Fig. 6. (a) Line drawing of plan view of model 2, and (b) some sequential profiles showing horst-graben structures with a reactive diapir after 20% bulk extension.

other at shallower levels in the sand layer as the brittle/ductile thickness ratio increased.

To minimise the boundary effect of the moving wall on model 4, a thin rigid plastic sheet, 10 cm in width and 30 cm in length, was attached to the moving wall (Fig. 12). This plastic sheet was placed horizontally between the rubber sheet and the model. Normal faults developed a concentrated rift zone above the edge of the rigid plastic (Fig. 12).

Profiles of model 4 above the FD half indicate that structures were inhibited both far from the moving wall and above the rigid plate attached to the moving wall, and concentrated to a single complex asymmetric graben above its edge (Fig. 12a). As the brittle/ductile thickness ratio increased in the DD half compared with model 2, symmetric horsts and grabens developed are most of the length of the model (Fig. 12b).
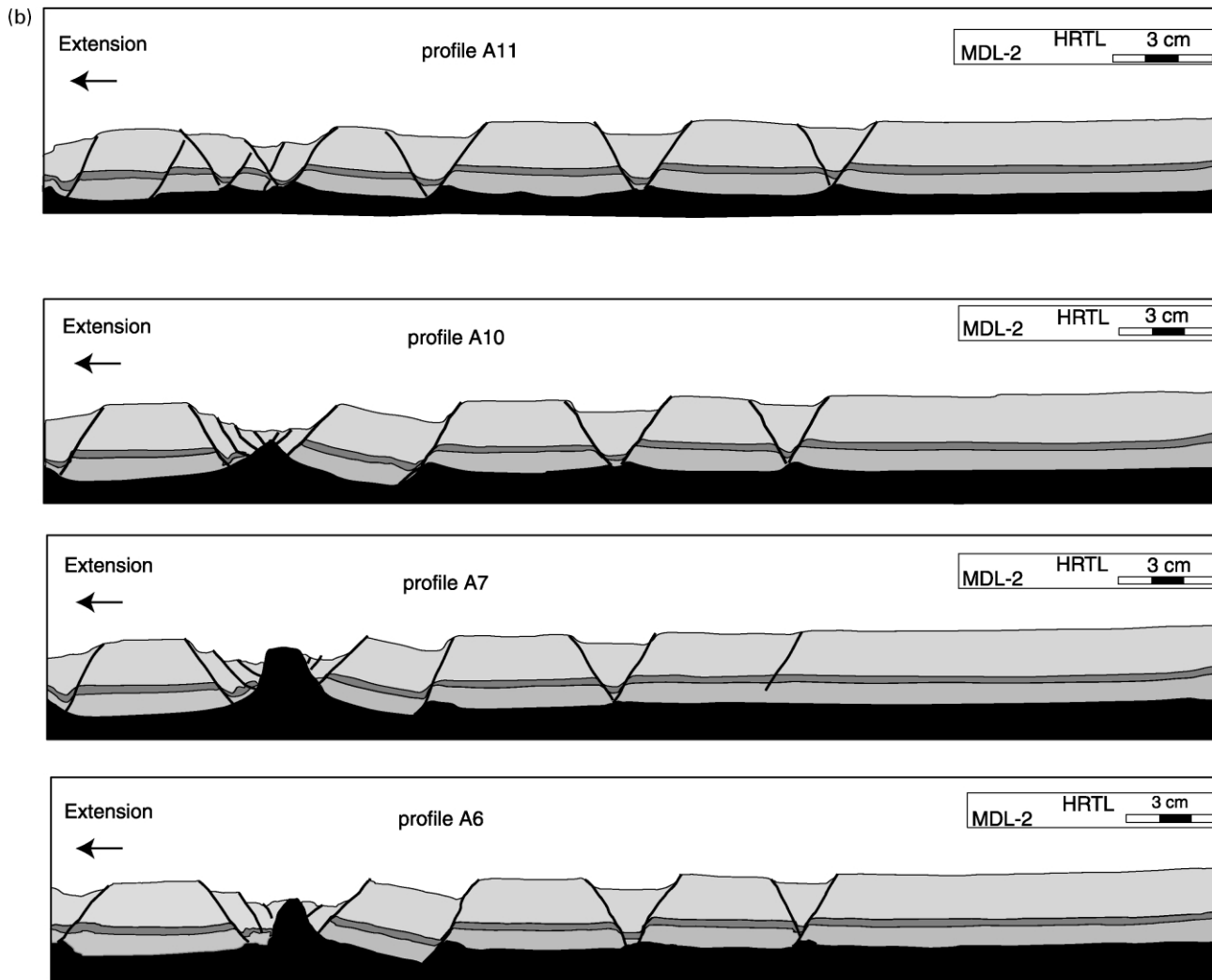
Fig. 6 (*continued*)

Model 5, with the boundary between the DD and FD halves oblique to the extension direction, shows similar structures to model 2 with the same brittle/ductile thickness ratio. A profile parallel to the extension direction (Fig. 9a), in the DD half of model 5 shows a regular sequence of horst and graben, as well as a reactive diapir close to the moving wall.

Model 8 was built by adding two layers (each 4 mm thick) of glass beads (300 μm in diameter) between sand layers to simulate an active lithological layering and to study the effects of mechanical stratigraphy. This model was extended to the same amount (20%) of bulk extension at the same displacement rate as the other models in this series (Fig. 13a and b). Profiles of the DD and FD halves of this model were identical to those of model 3 (Fig. 7a and c) without any mechanical layering; no visible fault developed in the FD half of model 8 after 20% bulk extension.

In model 11, the glass beads simulated a low frictional strength detachment beneath the sand layer. Profiles of the LFD half show the horst and graben expected from other models. However, profiles of the LFD half show some normal faults with small displacements restricted to profiles close to the boundary between the DD and LFD halves (Fig.14a). These faults can be attributed to the effect of faulting in the DD half propagating into the LFD half. However, no visible faults occur along the middle of the LFD half (Fig. 14b).

Normal faults characterised the sand layer extended above the DD halves of most models. By contrast, faults in the FD halves developed only close to the moving wall and can be attributed to boundary effect (Figs. 6a, 7b and 8a). Extension of the sand layer above the DD was shared between translation along faults and penetrative strain. Measurement of the initial and final length of the sand layer extended above a DD indicates penetrative strain in all sand layers extended above a DD was less than 10%, except in model 9, which had no ductile substrate.

Table 3 lists measurements of translation, penetrative strains and the number of faults and their mean dips in all profiles recovered from model 3 as an example of our
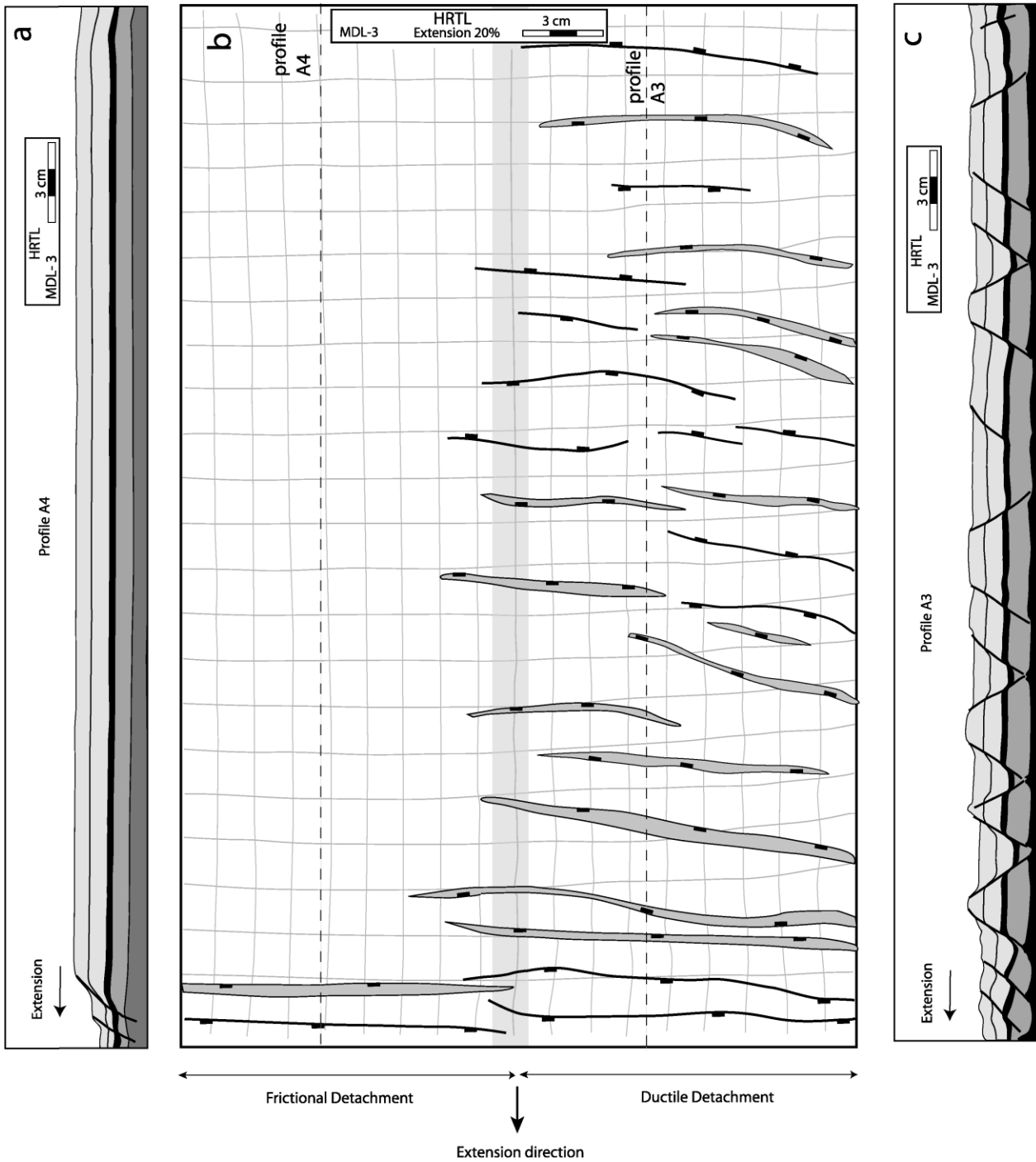
Fig. 7. (a) Line drawing of two profiles ((a) and (c)) and plan view (b) of model 3 after 20% extension above the rubber sheet: (a) profile across the FD half showing homogeneous extension of sand layers, (b)plan view showing development of normal faults in the cover above the DD half, and (c) profile across the DD half showing horst and graben structures.

analyses of all models. In the FD halves, the vast majority of extension (about 90% of total bulk extension) above the stretched rubber sheet was accommodated by penetrative strain and uniform thinning of the sand layer. As a consequence, the amount of penetrative strain changes from 8 to 12.26% in different profiles through the DD half.

In profiles parallel to the extension direction of model 9,

the faults show a domino pattern (Fig. 11). The right-lateral synthetic normal fault sets generally dip toward the extension direction. Their profiles are sigmoidal and subplanar with displacements that generally decrease from top to bottom. In the 3-cm-thick sand layer, the faults have constant spacing of 7.5–8.5 mm. Sand blocks are rotated by $14°–15°$ relative to the horizontal.
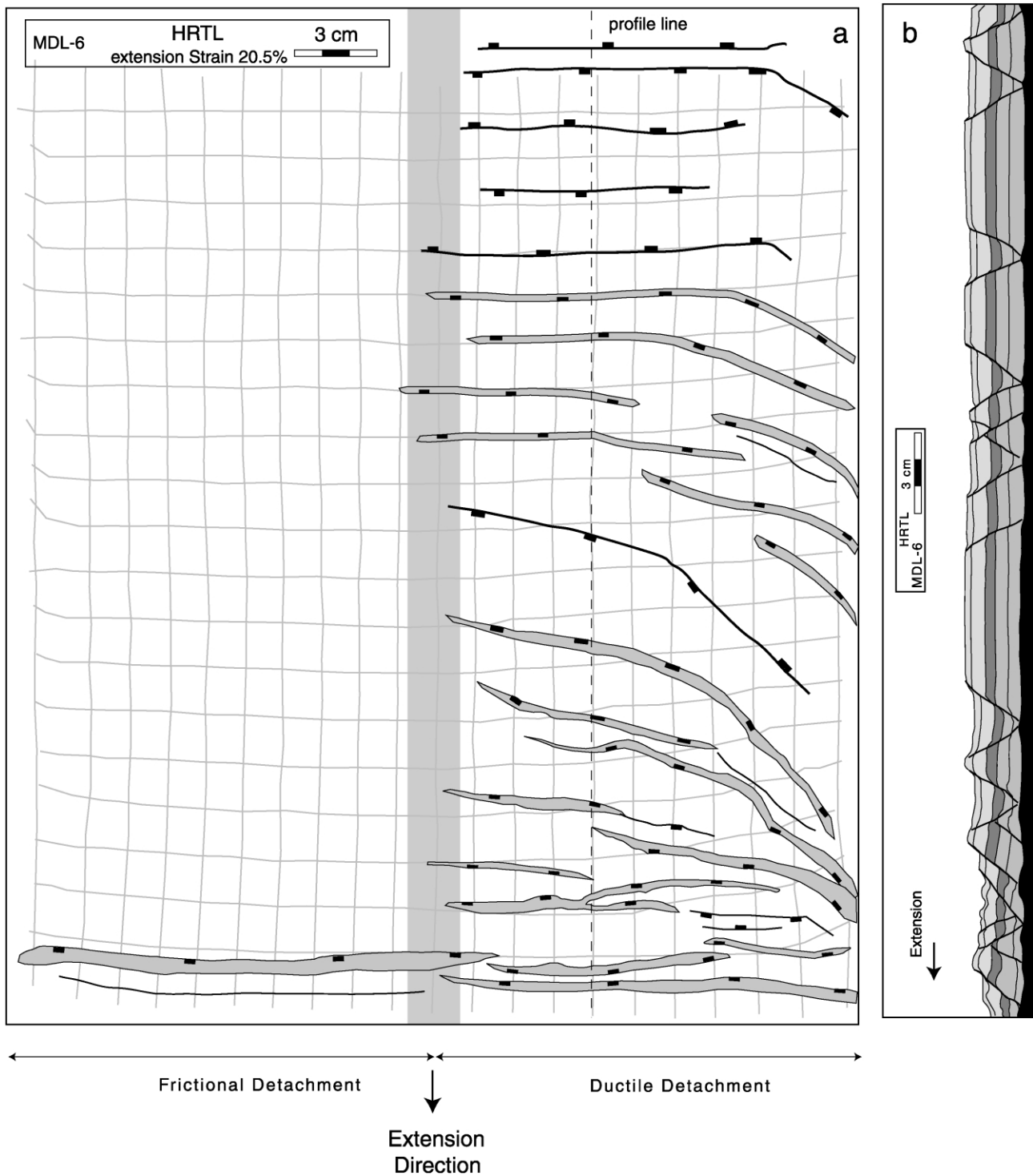
Fig. 8. (a) Line drawings of plan view of model 6 showing development of the normal faults over the DD half, and (b) profile across the DD half showing a series of structures including horst-graben and half graben after bulk extension of 20.5%.

5. Discussion

The mechanisms of lateral extension in the models presented here related strongly to the nature of the detachment and the ratio between the thicknesses of the brittle overburden and any ductile substrate. Below, we discuss these parameters.

5.1. Episodic and continuous extension

Extension by unfolding of a banded basal sheet was localised to a narrow zone in the overlying sand in models 1 and 7. With progressive extension, the rigid strips were separated one by one, then focussing extension to a narrow zone that migrated away from the moving wall in small
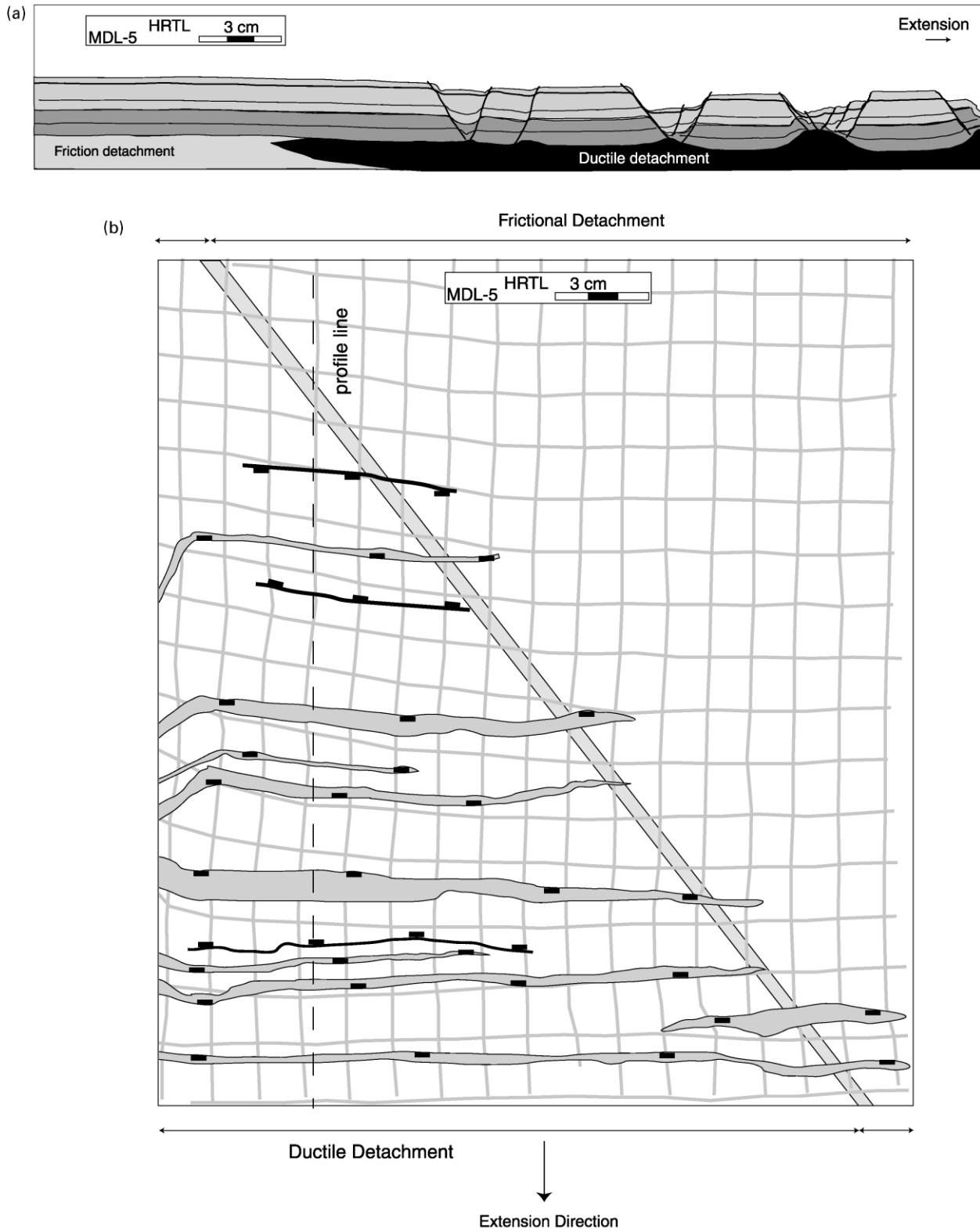
Fig. 9. (a) Profile and (b) plan view of model 5 showing oblique distribution of the DD and the FD to extension direction. Development of structures restricted above the DD and their lateral propagation was controlled by the boundary between two halves.
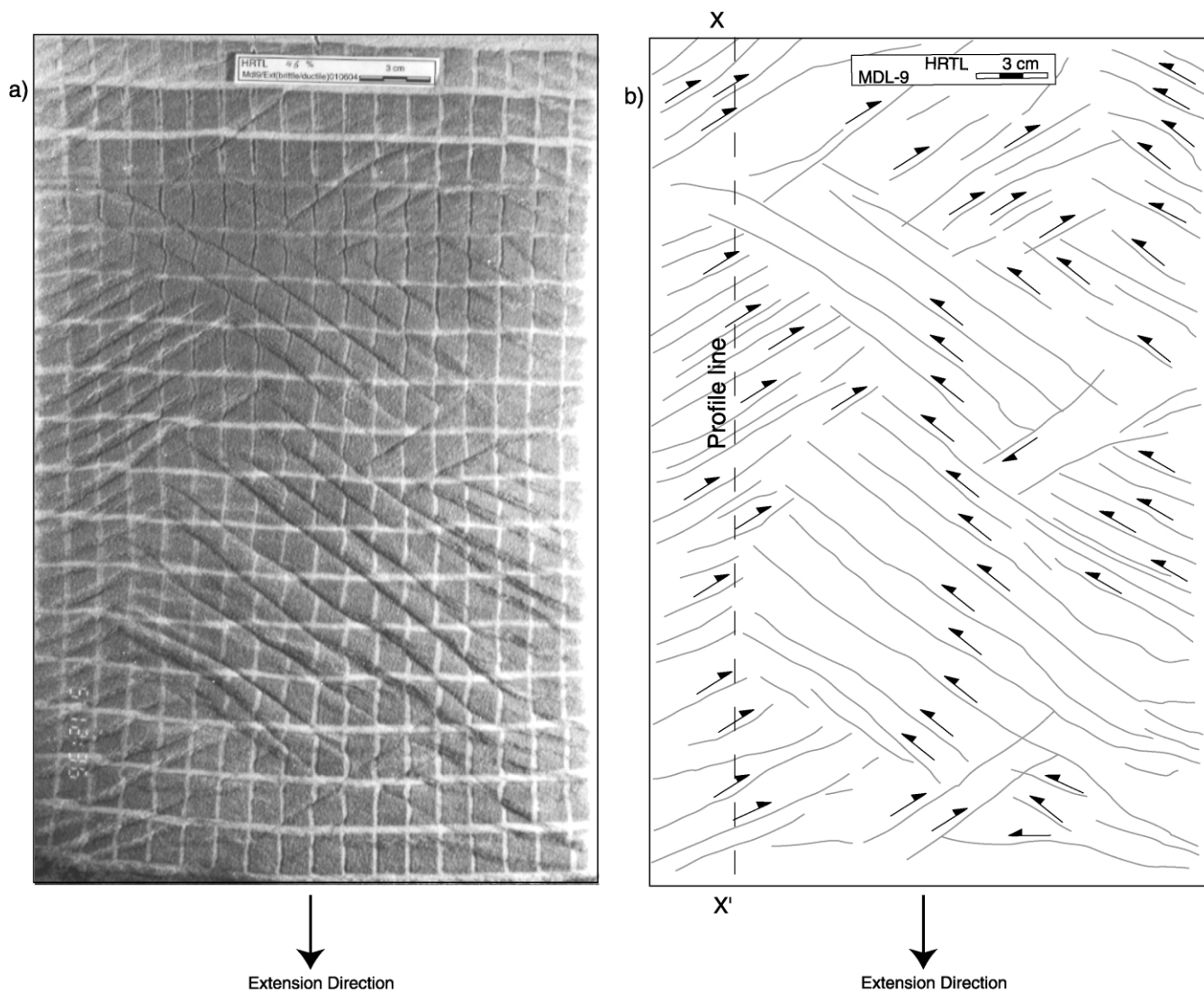
Fig. 10. (a) Photograph and (b) line drawing of plan view of model 9 after bulk extension of 46% showing conjugate set of faults, which have oblique slip consisting of strike and dip-slip components.

Table 3
Proportions of translation and penetrative strain in model 3

| Profile	Basal substrate	Total bulk extension (%)	Translation extension (%)	Penetrative extension (%)	Number of fault	Mean dip of faults
Ductile Decollement Half						
Profile A1	Silicon	20.00	10.70	9.30	10	55
Profile A2	Silicon	20.00	9.50	10.50	14	58
Profile A3	Silicon	20.00	11.50	8	13	57
Profile A4	Silicon	20.00	7.74	12.26	13	51
Profile A5	Silicon	20.00	8.10	11.90	13	60
Profile A6	Silicon	20.00	8.36	11.64	18	60
Frictional Decollement						
Profile A7	Sand	20.00	0	20.00	0	0
Profile A8	Sand	20.00	0	20.00	0	0
Profile A9	Sand	20.00	0	20.00	0	0
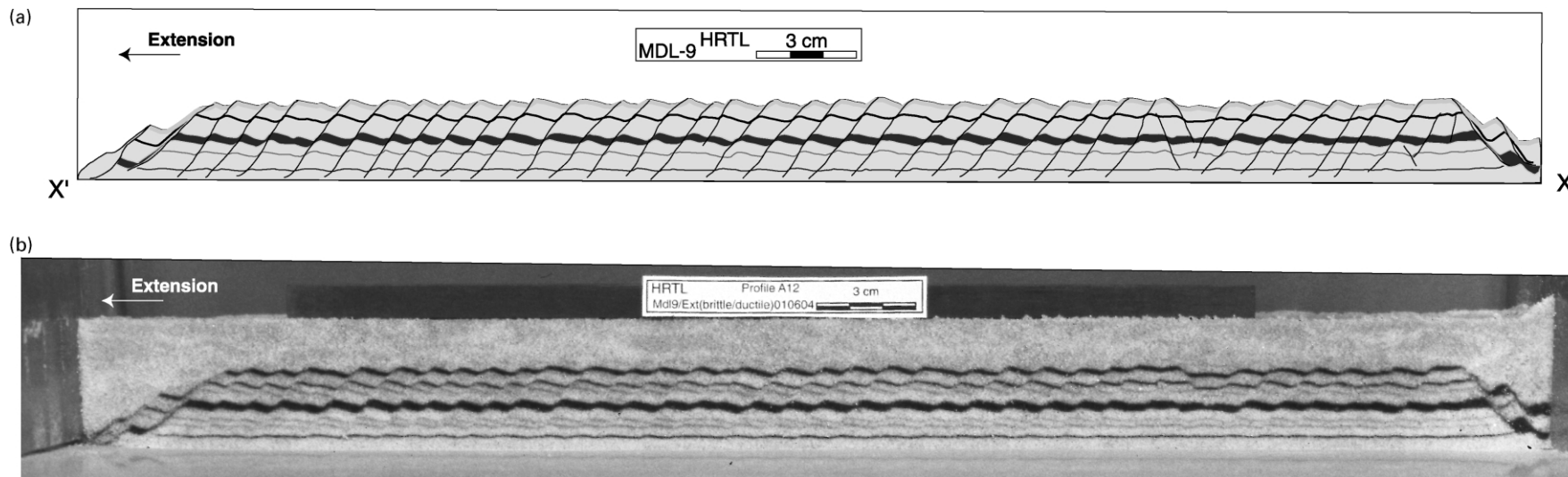
Fig. 11. (a) Photograph and (b) line drawing of profiles of model 9 cutting parallel to the extension show development of domino style of normal fault after 46% extension.
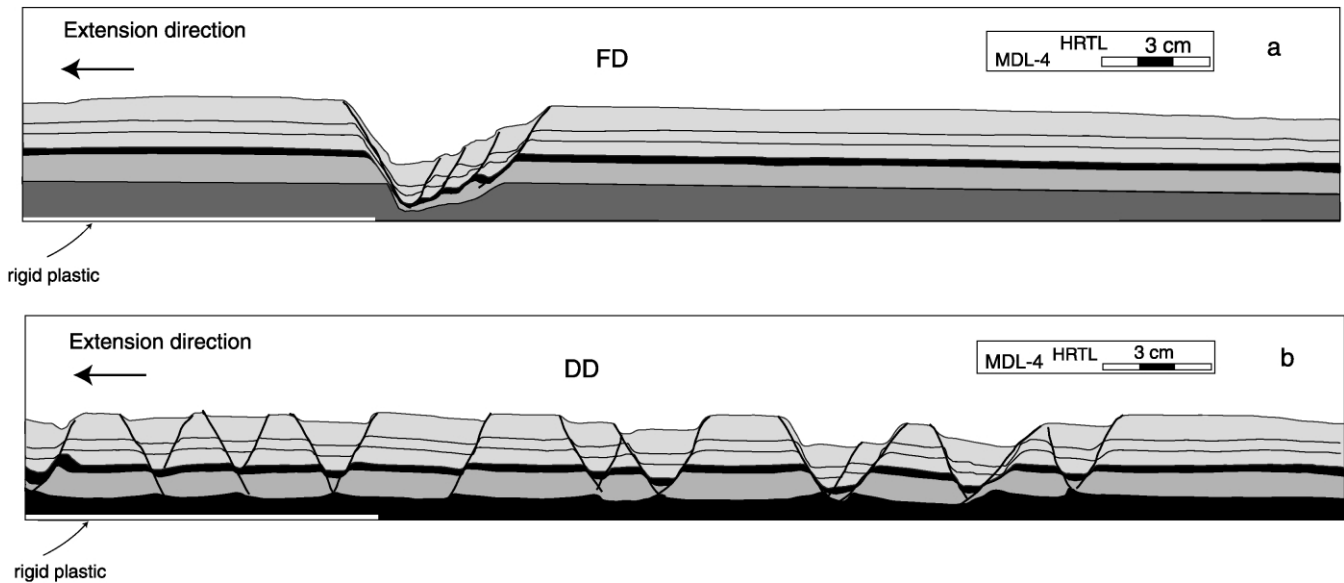
Fig. 12. (a) Line drawing of profiles of model 4 above the FD half showing an asymmetric rift formed and edge of a basal thin rigid plastic, and (b) profile across the DD half where horst and graben propagated throughout the model after bulk extension of 19.5%.

increments. As a result, separation of any two adjacent plastic strips controlled nucleation, propagation and spacing of normal faults in the overlying sand layers (Figs. 4 and 5). These active stripes simulate the role of basement normal faults that produce heterogeneous extension. Previous physical modelling of the effect of pre-existing normal faulting reactivating in the basement showed that extension, in the absence of a viscous layer between the basement and its cover, is generally concentrated above a master normal fault (Horsfield, 1977; Richard, 1990; Withjack and Callaway, 2000). Similarly, in profiles of models 1 and 7 (Figs. 4b and 5a), faults extrapolate down to the edges of rigid strips with a one to one correlation and conjugate sets intersected each other at shallow level within the sand layer above the FD halves (Figs. 4b and 5a). By contrast, there is no such correlation between active strips and faults formed in the sand layer developed above the DD halves (Figs. 4d and 5c). This observation matches earlier reports of previous physical models in which brittle covers extended over viscous layers did not develop normal faults immediately above active faults in the basement (see Fig. 4b and d; Vendeville, 1987; Richard, 1990, 1991; Bobineau 1992; Koyi et al., 1993; Withjack and Callaway, 2000).

There have been many previous studies of sand or clay layers extended homogeneously above a rubber sheet in deformation rigs similar to that used in this study (e.g. Cloos, 1955; McClay and Ellis, 1987a,b; Vendeville et al., 1987; Mandl, 1988; McClay, 1990; Ishikawa and Otsuki, 1995; Keep and McClay, 1997; Kerr and White, 1996). There was no ductile substrate between the rubber sheet and the sand layer, in the DD half of our models. In equivalent circumstances, previous workers reported development of domino faults, whereas others reported sequential development of horst and graben in sand layers extended over 46%

above rubber sheets. By contrast, no faults developed in the FD half of our models 2, 3, 5, 6, 8 and 10 extended homogeneously. Model 8 (Fig. 13b) was designed to study the effect of homogeneous thin-skinned extension of horizontal layers of different mechanical strength, for example sandstone interbedded with beds of shale. Fig. 13b shows that no normal faults formed in the FD half containing layers of glass beads after 20% of bulk extension. In contrast, sequential horst and graben developed just above the DD similar to those in model 3 with the same brittle/ductile thickness ratio after the same amount of bulk extension (see also Fig. 7c).

This result suggests that mechanically active horizontal layering is insufficient to initiate normal faults in covers extended above smooth frictional décollements. Thus, results of our model 8 confirm recent results of numerical models by Harper et al. (2001) who also found that no faults developed in mechanically layered models. Other numerical models by the same workers (Harper et al., 2001, fig. 1a) found that frictional cover sequences uniformly extended above frictional décollements do uniformly thin without significant faulting. These models led Harper et al. (2001) to argue that the development of well-defined extensional faults in the cover requires heterogeneities in either the cover or the basement (the latter having been confirmed in the FD halves of our banded-base 'faulted basement' models).

The homogeneous extension and delay in faulting until >20% bulk extension in the FD halves of our models 2, 3, 5, 6, 8 and 10 strikingly confirms the results of Harper and co-workers' (2001) numerical models and indicates analogue extension models.

The sand layer in model 9 appeared to extend uniformly above the rubber sheet even after 20% bulk lateral extension
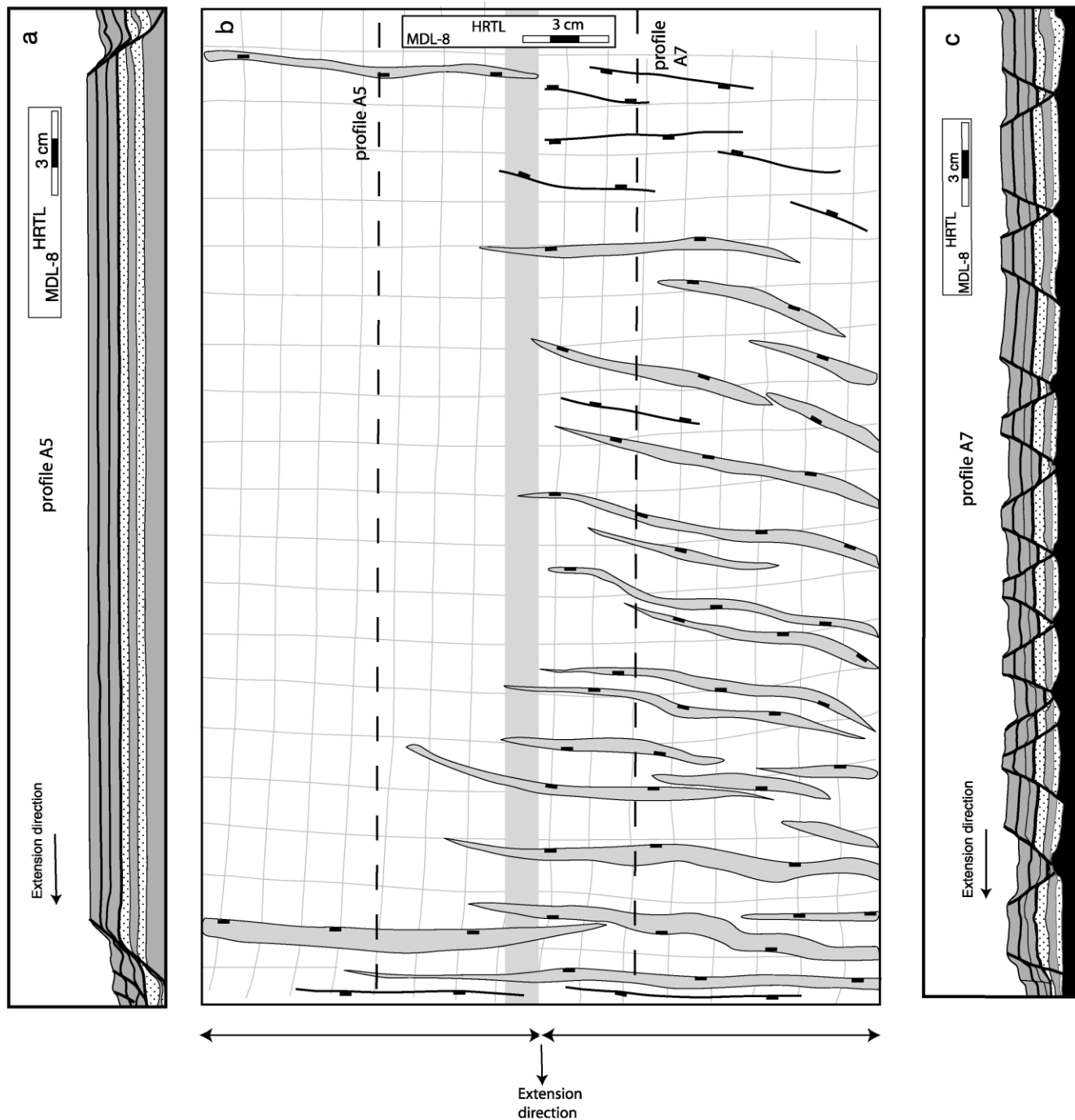
Fig. 13. Line drawing of two profiles ((a) and (c)) and plan view (b) of model 8 consist of the sand layers with interbeds of glass beads (dotted) for simulating different mechanical properties: (a) profile of the FD half showing homogeneous extension of sand and glass bead layers, (b) plan view of the model showing development of normal fault above the DD half, and (c) profile along the DD half showing development of sequential horst and graben after 20% bulk extension.

(i.e. any structures formed were below the resolution of the sand grains) Our rubber sheets were nominally extended uniaxially but in fact increasingly deformed by biaxial strain and narrowed as they extended as in previous analogue models. The two conjugate sets of obvious faults that developed beyond 20% bulk extension are attributed to increasing biaxial strain introduced by shortening of the rubber sheet perpendicular to the extension direction

(Figs. 10 and 11) as recognised by previous workers who extended models over rubber sheets (e.g. McClay and Ellis, 1987a,b; McClay, 1990). McClay (1990) showed regular domino-style faults similar to those in Fig. 11. We attribute the differences between our results and those results of McClay and Ellis (1987a,b) and McClay (1990) not to the design of the deformation rig, but merely to that they were adding growth sediments to their models during extension.
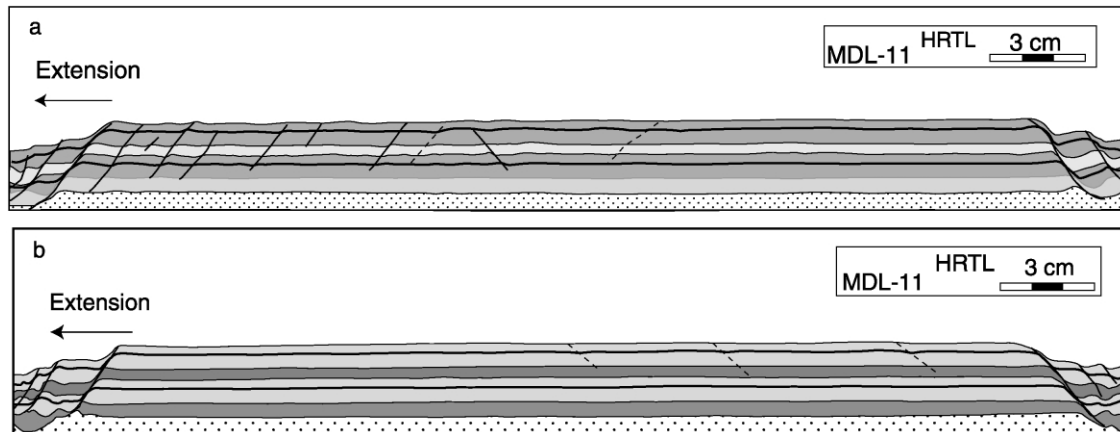
Fig. 14. Line drawing of two profiles of the low friction detachment from model 11 after 20% bulk extension. (a) Profile along the LFD half close to boundary of the DD half and the LFD half showing formation some normal faults with small amounts of displacement, and (b) profile at middle of the LFD half showing homogeneous extension of the sand layer, except beside the moving and fixed walls.

Syn-kinematic sedimentation in previous studies may have obscured the top view expression of faults. In our study, the top view of the models remained exposed throughout extension. This is, that sand covers extend above frictional décollements by thinning uniformly and homogeneously up to 20% bulk extension. Thereafter, they develop two rotating suites of conjugate faults oblique to the extension direction, which simulate domino or book-case faulting in profiles parallel to the extension direction (see Figs. 10 and 11). These faults possess both strike- and dip-slip components.

The difference between our model results and those of Vendeville et al. (1987), who did not add growth sediment to their models, may be attributed to the design of the deformation rig, which may have led to heterogeneous extension in this model. Harper et al. (2001) also suggested heterogeneity to be the explanation for such a difference. However, we do not know the exact reason for this difference.

5.2. Influence of detachment

The models presented here explore the effect of ductile and high-frictional detachments above two different basal configurations, which lead to step-wise and homogeneous extension. Our results indicate that the reactivation of basement faults below the detachment can control the style and rate of extension in the overburden.

Since the banded sheet gives rise to simultaneous development of normal faulting in both the DD and FD halves of models 1 and 7, which differed in brittle/ductile thickness ratio, it was not possible to distinguish the effect of the frictional and ductile detachments on their modes of deformation. Nevertheless, the following differences between the FD and DD halves of these models are obvious:

1. Extension occurred in a deformation zone that was wider (28–32 mm) above the DD than above the FD (21–28 mm) (see Figs. 4 and 5)

2. Normal faults were more numerous above the DD ($\sim$15–19) than above the FD ($\sim$26–28). Faults developed above the FD are longer and straighter in map view.
3. Minor or second generation normal faults are fewer above the DD than the FD.
4. Normal faults deflect, overlap and terminate in the boundary zone between the FD and DD halves (see Figs. 4c and 5b). This boundary represents a transfer or accommodation zone with relay ramps between faults. The propagation rate of basal extension was 0.96×10^{-3} cm s^{-1} in the FD and 1.4×10^{-3} cm s^{-1} in the DD half.

Profiles of the FD halves of models 1 and 7, show that normal faults developed in two conjugate sets with intersection angles of about 60° (Figs. 4b and 5a). Displacement on these conjugate normal faults was not necessarily simultaneous as many of them crossed and offset earlier faults. Some earlier normal faults were reactivated and offset by new faults as also described by Horsfield (1980) and Ferrill et al. (2000).

Normal faults developed above a FD generally intersect near the middle of the sand layer in profile (Figs. 4b and 5a). Faults above the DD intersect at the base of the sand layer or just below graben. Grabens are wider above a DD than those above a FD.

In contrast to step-wise extension, homogeneous extension above a rubber sheet was entirely uniform and homogeneous above the FD halves of models 2, 3, 5, 6, 8, 10 and 11. The frictional coupling between the rubber sheet and the overlying sand layer was sufficient to lead to uniform and homogeneous layer-parallel extension up to bulk extension of 20%. The glass beads used as a low frictional detachment in model 11 decreased the coupling between the rubber sheet and the overlying sand layer. A result, some normal faults with small displacement developed locally in the LFD half of model 11 (Fig. 14).Nevertheless, the

heterogeneity introduced into the base of the FD half by adding a thin rigid plastic to the moving wall in model 4 (see Table 1) led to localised faulting in the sand layer.

Models 2–6, 8, 10 and 11 showed that a DD can lead to structures in the sand layer by homogeneous extension similar to those formed in step-wise extension. Increasing the thickness ratio in models 2, 3 and 6 (see Table 1 and Figs. 6b, 7c and 8b) increased the number and dip of normal faults and the width of the deformation zone. Model results show that there is an inverse relationship between the thickness of the ductile substrate and the number of faults formed in the overlying layers. As the thickness of the ductile substrate decreases (e.g. models 6, 8 and 10) the number of faults formed in the overlying layers increase and vice versa (Fig. 15). At brittle/ductile thickness ratios >4, the sand layer developed mixtures of horst, graben, and half-graben (Fig. 8b). By contrast, low brittle/ductile thickness ratios resulted in a regular pattern of horst and graben with or without re-active diapirs (see Fig. 6b). The spacing of the horst or graben is controlled by the thickness ratio. Increasing the brittle/ductile thickness ratio decreases the spacing of normal faults (compare Figs. 6b and 7c).

5.3. Strain partitioning

Thin-skinned extension in uniaxially extended sand covers was accommodated by normal faulting, block rotation and penetrative strain due to change in packing of the sand. The latter is represented by uniform elongation or layer-parallel extension that thins the marker layers (see Means, 1976). Similarly, in our models, penetrative extension resulted in bulk thinning of the deformed sand layers. The ratio of extension by penetrative strain and faulting varied both between different models and the two halves of the same model.

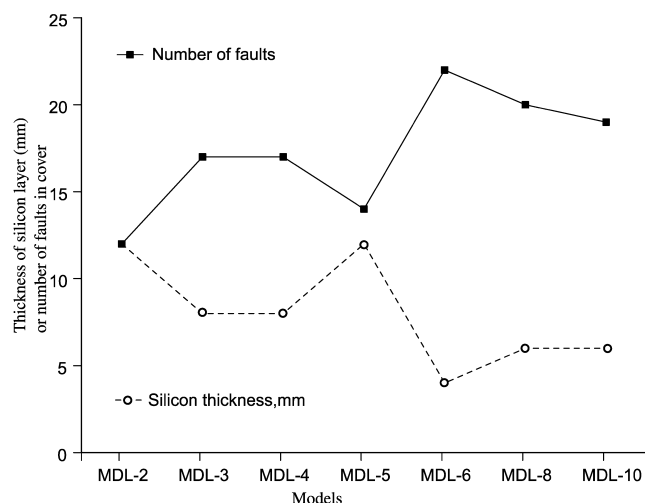Where normal faults developed in models 1 and 7, which

Fig. 15. Plot showing relation between number of faults and thickness of the ductile substrate in different models extended above the rubber sheet.

were extended step-wise (see Figs. 4 and 5), the extension due to faults in the DD halves was generally <10%, whereas it was nearly 100% in the FD halves.

By contrast, bulk extension was penetrative (layer-parallel extension) in the FD halves of model 2, 3, 5, 6, 8, 10 and 11. Bulk extension in the FD half of model 4 concentrated to a graben. By contrast, bulk extension was fault extension and penetrative strain in different proportions in the DD halves of models 2–6, 8, 10 and 11 (see Table 3). Measurements of square markers initially marked on the surface of the model revealed that penetrative extension was close to zero above the FD in models 1 and 7 extended above a banded sheet, whereas it was up to ∼10% above the DD half (see also Benes and Davy, 1996).

Along-strike segmentation of normal faults has been attributed to heterogeneous distribution of displacements along fault surfaces or systems of fault surface (Figs. 4c, 5b, 7b and 8a; Roberts and Yielding, 1990; Faulds and Varga, 1998). In plan view, the traces of many normal faults above a DD are offset in en-échelon fashion with associated overlapping zones. In models 1 and 7, the faults were offset along the boundary between the DD and FD halves. Normal faults were both hard-linked by transfer faults and soft-linked by relay ramps in different parts of model 1, 7, 3 and 6 (Figs. 4c, 5b, 7b and 8a).

6. Geological implications

Thin-skinned extension of cover sequence above eva-porites (mainly salt) has been recognised on seismic profiles and geological surveying in many regions around the world (Fig. 16; Jackson and Talbot, 1990; Vendeville and Jackson, 1992). Evaporitic substrates act as ductile detachments and after die out laterally to non-evaporitic frictional detachments (FD). Horst and graben with or without diapiric structures resembling our models extended above a DD have been reported from many regions, for example the North Sea, Gulf of Suez and Red Sea. One of the best examples for sequential development of horst and graben above a ductile décollement is the Canyonlands National Park, Utah (Fig. 16b) where the Paradox formation provides a ductile décollement for the brittle overburden consisting of sandstones and limestones (McGill and Stromquist, 1979; Schultz-Ela and Walsh, 2002). Similar to profiles of model 2 and 3 extended above a ductile décollement (Figs. 6b and 7c), grabens in the Canyonlands have constant spacing. By contrast, we know of no reports from nature of frictional overburdens uniformly extended above a FD as in our analogue models and the numerical models of Harper et al. (2001). Any natural examples would be difficult to detect, especially on seismic profiles. Any homogeneous lateral extension in nature is unlikely to be recognised because, unlike models, final thickness cannot be compared with initial thickness. Any such penetrative extensions in nature may be manifested by closely spaced subvertical dilation
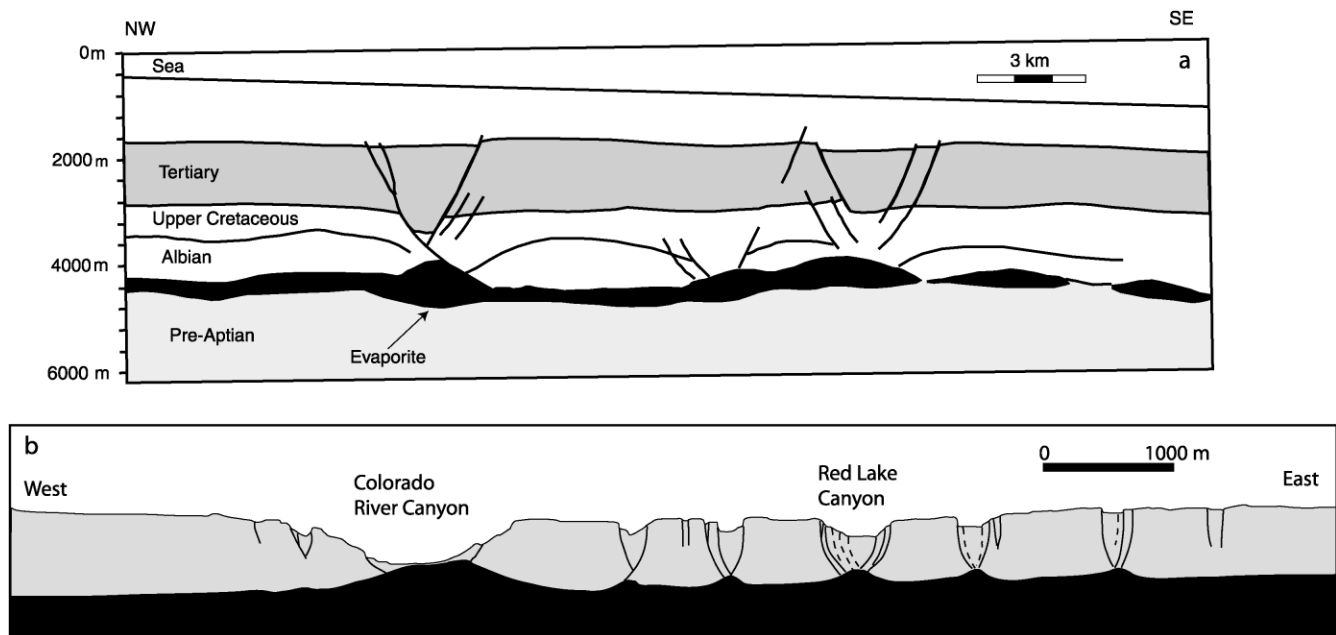
Fig. 16. (a) Line drawing of seismic section across Brazilian continental margin show development of graben structures above the ductile detachment (DD) after Cobbold et al. (1989), and (b) line drawing of a cross-section of the Canyonlands of the National Park, Utah after Schultz-Ela and Walsh (2002).

fractures close to perpendicular to the extension direction. Thus, penetrative strain may be accompanied by: (a) closely spaced dilation fractures perpendicular to the extension axis, (b) two conjugate sets of steep strike-slip surface bisected by the extension direction, and (c) subhorizontal bedding-parallel slip surfaces (with/without slicken lines).

However, detaching on Jurassic sediments is found in large parts of the Barents Sea. The Jurassic sediments that the faults sole into are neither cut by deeper faults nor are evaporitic in nature. For example, Cretaceous and lower Tertiary units in the Nordkapp Basin of the Barents Sea are intensively faulted by small-scale, closely spaced faults terminating near the base Cretaceous unconformity (Fig. 17a and b). The throw on the faults is generally less than 20 ms (TWT), (Richardsen, 1991). The intensity of these faults in the Nordkapp basin is less (five faults per 10 km) relative to other areas in the Barents Sea (e.g. Bjermeland and Finnmark platforms), where the intensity is twice as much (10 faults per 10 km). These faults have been related to halokinetic readjustment due to salt movement (Bergendal, 1989). However, the location of these faults (some are present in areas far from any diapiric influence), the fact that they are most of them terminate at the base Cretaceous unconformity and that they neither radial not concentric to the diapiric structures questions their origin to be related to diapiric movements. We attribute these closely spaced faults to regional extension during the tectonic episodes in Early Cretaceous and Tertiary times that reactivated some of the basins (Gabrielsen et al., 1990). However, towards the end of Cretaceous, regional extension may have prevailed in the Barents Sea. The extension was probably accommodated by the large marginal faults in the basins. However, in areas where large faults were absent, the extension was accommodated by closely spaced faults, which probably decoupled

from older units (Jurassic and older) and sole to the base Cretaceous unconformity. Some of these faults with larger throws (>20 m) cut down into Triassic units. We compare the closely spaced fault population in the Barents Sea to those closely spaced dilation fractures and fissures formed above the frictional décollement in model 2 (Fig. 6a).

7. Conclusions

The models presented here indicate that the mechanical characteristics of detachments play a significant role in controlling the mode and rate of deformation and thus the style of thin-skinned extension (Table 4). Step-wise deformation propagates faster and further above a ductile detachment in plan view, whereas it is more localised above a frictional detachment. If there is no ductile substrate beneath an extended cover sequence, old faults reactivated in the basement nucleate normal faults in the base of the overlying cover. Correlation between discrete faults in the basement and more dispersed faults in profiles of the cover is poor where a ductile detachment decouples the two units. Our models imply that apparently undeformed flat-lying rock sequence may in fact have laterally extended above frictional detachments homogeneously and cryptically by penetrative bulk strain.

Rheological differences between ductile and frictional décollement in adjacent areas can lead to deformation gradients that result in different patterns of normal faults with both hard and soft linkages.

In our models extended above the rubber sheet, stretching in one direction produced shortening at right angles. Such biaxial strain beyond 20% of bulk extension led to the
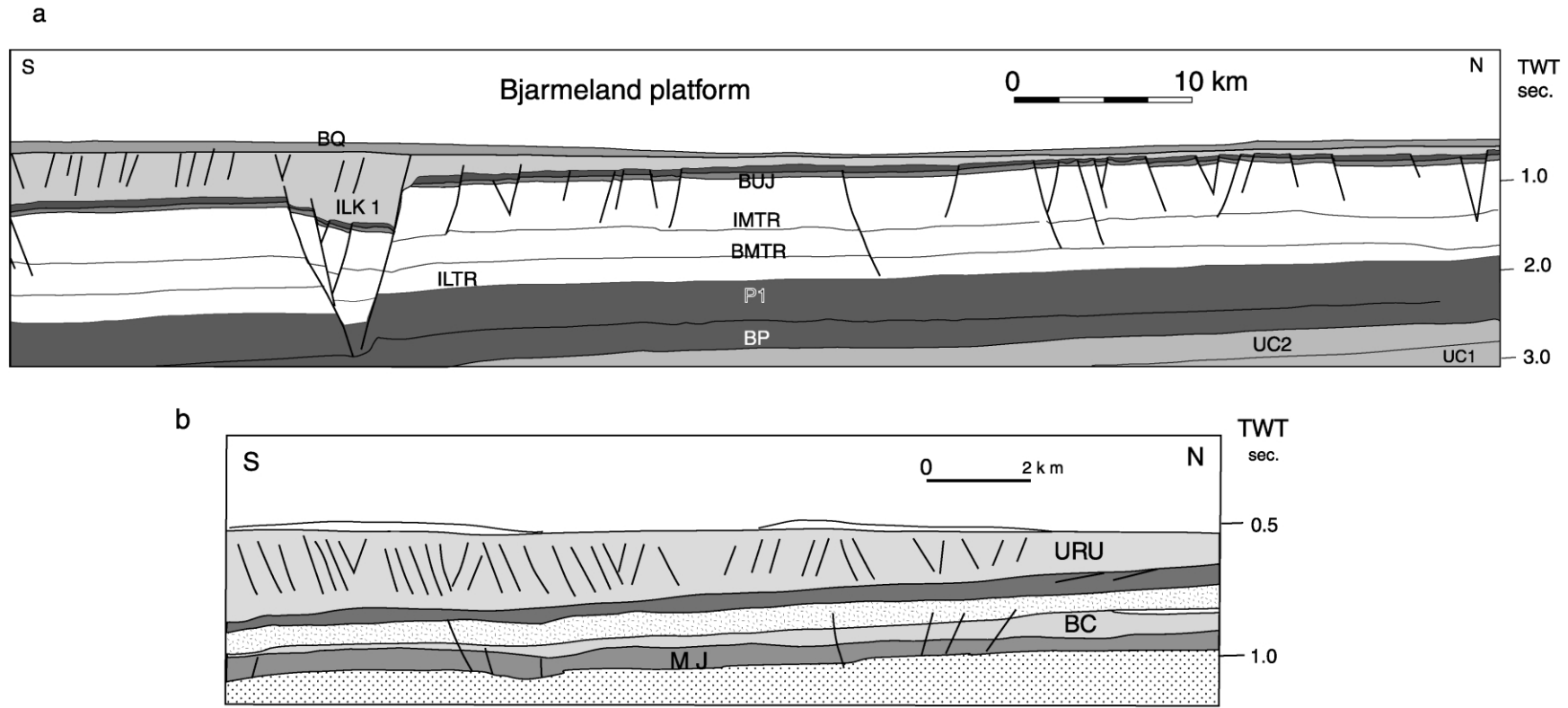
Fig. 17. (a) Line-drawing of a seismic section from the Bjarmeland platform showing closely-spaced small-scale normal faults in Creataceous sediments (ILK1) in the southern side and large-scale faults in Triassic sediments (BMTR and IMTR) in the northern side of the section. The Bjarmeland platform represents the stable area, consisting of small scale faults above Paleozoic (UC[//]: late Carboniferous, top of salt UC1; BP: near base of Permian; P1: near top of Permain; Meszosoic: BMTR: base of Middle Triassic; IMTR: Middle Triassic; BUJ: base of Upper Jurassic; ILK1: intra low Cretaceous; and BQ: Quaternary). (b) Seismic section from the Nordkapp Basin showing closely-spaced small-scale faults in Cretaceous and Tertiary sediments (MJ: Middle Jurassic; BC: base of Cretaceous; URU: upper regional unconformity).

Table 4
Summary table of model results

	Ductile Decollement		Frictional Decollement	
Heterogeous Extension (Stepwise)	*Low* ← **Brittle/Ductile ratio** → *High*		*Low* ← **Over burden Thickness** → *High*	
	Few normal faults	More normal faults	Very closely spaced, longer and straighter normal faults, regular horst & graben	Closely spaced normal faults irregular horst & graben
	Narrow deformation zone	Wide deformation zone		
	Reactive diapir	No reactive diapir		
	Block Rotation		No Block Rotation	
	Fault intersection at top of the ductile layer		Fault intersection in the frictional over burden	
	Pentrative Strain		No Pentrative Strain	
Homogeneous Extension	*Low* ← **Brittle/Ductile ratio** → *High*		*Low* ← **Mechanical Strength** → *High*	
	Few Normal faults	More Normal faults	Few Normal faults dilation fissures	No Normal faults, dilation fissures
	Widely spaced horst & graben	Closely spaced normal faults or horst & graben		
	Penetrative Strain < 13%		Penetrative Strain > 90 %	
	No effect by mechanical stratigraphy		No effect by mechanical stratigraphy	

development of two conjugate sets of steep faults both dipping 68–76° towards the extension direction with both dip and strike slip displacements. We suspect that many previous illustrated causes of simple book-case faulting seen in cross-sections of models or on seismic profiles actually involved two suites of conjugate faults in plan view.

Acknowledgements

References

Benes, V., Davy, P., 1996. Modes of continental lithospheric extension: experimental verification of strain localization processes. Tectonophysics 254, 69–87.

Bergendal, E., 1989. Halokinetisk utvikling av Nordkappbassenhets sørvestre segment. Unpublished candidate scientific thesis. Department of Geology, University of Oslo.

Bobineau, J.P., 1992. Simulations numeriques de phenomenes tectoniques. These de L'Ecole Centrale de Paris.

Brace, W.F., Kohlstedt, D.L., 1980. Limits on lithosphere stress imposed by laboratory experiments. Journal of Geophysical Research 85, 6248–6252.

Brun, J.P., Choukroune, P., 1983. Normal faulting, block tilting and décollement in a stretched crust. Tectonics 2, 345–356.

Brun, J.P., Choukroune, P., Faugéres, É., 1985. Les discontinuités significantives de l' amincissement crustal: application aux marges passives. Bulletin de la Société Géologique de France 8, 139–144.

Byerlee, J., 1978. Friction of rocks. Pure Applied Geophysics 116, 615–625.

Chapple, W.M., 1978. Mechanics of a thin-skinned fold-and-thrust belt. Geological Society of American Bulletin 89, 1189–1198.

Childs, C., Watterson, J., Walsh, J.J., 1995. Fault overlap zones within developing normal fault systems. Journal of Geological Society, London 152, 535–549.

Cloos, E., 1955. Experimental analysis of fracture pattern. Geological Society of America Bulletin 66, 241–256.

Cobbold, P.R., Rossello, E.A., Vendeville, B., 1989. Some experiments on interacting sedimentation and deformation above salt horizons. Bulletin de la Société Géologique de France 8, 453–460.

Colletta, B., LeQuellec, P., Letouzey, J., Moretti, I., 1988. Longitudinal evolution of Suez rift structures (Egypt). In: LePichon, X., Cochran, J.R. (Eds.), The Gulf of Suez and Red Sea Rifting. Tectonophysics 153, pp. 69–87.

Cotton, J.T., Koyi, H.A., 2000. Modeling of thrust fronts above ductile and frictional detachments: Application to structures in the Salt Range and Potwar Plateau, Pakistan. Geological Society of America Bulletin 112, 351–363.

Davis, D.M., Engelder, T., 1985. The role of salt in fold-and-thrust belts. Tectonophysics 119, 67–88.

Davis, D.M., Engelder, T., 1987. Thin-skinned deformation over salt. In: Lerche, I., O'Brien, J.J. (Eds.), Dynamical Geology of Salt and Related Structures, Academic Press, pp. 301–337.

Faulds, J.E., Varga, R.J., 1998. The role of accommodation zones and transfer zones in the regional segmentation of extended terranes. Geological Society of America Special Paper 323, 1–45.

Ferrill, D., Morris, A.P., Stamatakos, J.A., Sims, D.W., 2000. Crossing conjugate normal faults. American Association of Petroleum Geologists Bulletin 84, 1543–1559.

Gabrielsen, R.H., Faerseth, R.B., Jensen, L.N., Kalheim, J.E., Riis, F., 1990. Structural elements of the Norwegian continental shelf, part I: the Barents Sea region. NDP Bulletin 6, 33.

Gaullier, V., Brun, J.P., Guerin, G., Leconu, H., 1993. Raft tectonics: the effects of residual topography below a salt décollement. Tectonophysics 228, 363–381.

Harper, T., Fossen, H., Hesthammer, J., 2001. Influence of uniform basement extension on faulting in cover sediments. Journal of Structural Geology 23, 593–600.

Horsfield, W.T., 1977. An experimental approach to basement-controlled faulting. Geologie en Mijnbouw 56, 363–370.

Horsfield, W.T., 1980. Contemporaneous movement along crossing conjugate normal faults. Journal of Structural Geology 2, 305–310.

Hubbert, M.K., 1937. Theory of scale models as applied to geologic structures. Geological Society of America Bulletin 48, 1459–1520.

Ishikawa, M., Otsuki, K., 1995. Effects of strain gradient on asymmetry of experimental normal fault system. Journal of Structural Geology 17, 1047–1053.

Jackson, M.A.P., Talbot, C.J., 1990. Advances in salt tectonics. In: Hancock, P.L., (Ed.), Continental Deformation, Pergamon Press, pp. 159–179.

Keep, M., McClay, K.R., 1997. Analogue modelling of multiphase rift systems. Tectonophysics 273, 239–270.

Kerr, H.G., White, N., 1996. Kinematic modelling of normal fault geometries using inverse theory. In: Buchanan, P.G., Nieuwland, D.A. (Eds.), Modern Developments in Structural Interpretation, Validation and Modelling. Geological Society Special Publication 99, pp. 179–188.

Koyi, H., 1988. Experimental modeling of role of gravity and lateral shortening in Zagros mountain belt. American Association Petroleum Geologists Bulletin 72, 1381–1394.

Koyi, A.H., Jenyon, M.K., Petersen, K., 1993. The effect of basement faulting on diapirism. Journal of Petroleum Geology 16, 285–312.

Koyi, H.A., Hessami, K., Teixell, A., 2000. Epicenter distribution and magnitude of earthquakes in fold-thrust belts: insights from sandbox models. Geophysical Research Letters 27, 273–276.

Krantz, R.W., 1991. Measurements of friction coefficients and cohesion for faulting and fault reactivation in laboratory models using sand and sand mixtures. In: Cobbold, P.R. (Ed.), Experimental and Numerical Modelling of Continental Deformation. Tectonophysics 188, pp. 203–207.

Kusznir, N.J., Roberts, A.M., Morley, C.K., 1995. Forward and reverse modelling of rift basin formation. In: Lambiase, J.J. (Ed.), Hydrocarbon Habitat in Rift Basins. Geological Society of London Special Publication 88, pp. 33–56.

Letouzey, J., Colletta, B., Vially, R., Chermette, J.C., 1995. Evolution of salt-related structures in compressional settings. In: Jackson, M.P.A., Roberts, D.G., Snelson, S. (Eds.), Salt Tectonics. A Global Perspective. American Association of Petroleum Geologists Memoir 65, pp. 41–60.

Lister, G.S., Etheridge, M.A., Symonds, P.A., 1987. Detachment faulting and the evolution of passive continental margins. Geology 14, 246–250.

Mandl, G., 1988. Mechanics of Tectonic Faulting, Elsevier, Amsterdam.

McClay, K.R., 1990. Extensional fault systems in sedimentary basins: a review of analogue models studies. Marine and Petroleum Geology 7, 206–233.

McClay, K.R., 1996. Recent advances in analogue modelling: uses in section interpretation and validation. In: Buchanan, P.G., Nieuwland, D.A. (Eds.), Modern Developments in Structural Interpretation, Validation of Modelling. Geological Society Special Publication 99, pp. 201–225.

McClay, K.R., Ellis, P.G., 1987a. Analogue models of extensional fault geometries. In: Cowards, M.P., Dewey, J.F., Handcock, P.L. (Eds.), Continental Extensional Tectonics, Geological Society Special Publication, 28, pp. 109–125.

McClay, K.R., Ellis, P.G., 1987b. Geometries of extensional fault systems developed in model experiments. Geology 15, 341–344.

McGill, G.E., Stromquist, A.W., 1979. The graben of Canyonlands National Park, Utah: geometry, mechanics, and kinematics. Journal of Geophysical Research 84, 4547–4563.

Means, W.D., 1976. Stress and Strain: Basic Concepts of Continuum Mechanics for Geologists, Springer-Verlag, New York.

Mulugeta, G., 1988. Modelling the geometry of coulomb thrust wedges. Journal of Structural Geology 10, 847–859.

Ramberg, H., 1967. Gravity Deformation and the Earth's Crust, 1st ed, Academic Press, London.

Ramberg, H., 1981. Gravity Deformation and the Earth's Crust, 2nd ed, Academic Press, London.

Ramsay, J.G., Huber, M.I., 1987. The Techniques of Modern Structural Geology, Academic Press, London.

Richard, P., 1990. Champs de Failles Audessus d'un Decrichement de sicle: Modelisation Expermentale. Ph.D. thesis, University of Rennes.

Richard, P., 1991. Experiments on faulting in a two-layer cover sequence overlying a reactivated basement fault with oblique-slip. Journal of Structural Geology 13, 459–469.

Richardsen, G., 1991. Cenozoic geology of the southwestern Barents Sea: an analysis of erosional and depositional history based on seismic data. Ph.D. thesis, University of Tromsø.

Roberts, A., Yielding, G., 1990. Continental extensional tectonics. In: Hancock, P.L., (Ed.), Continental Deformation, Pergamon Pres, pp. 223–250.

Schlische, R.W., 1995. Geometry and origin of fault-related folds in extensional settings. American Association Petroleum Geologists Bulletin 79, 1661–1678.

Schultz-Ela, D.D., Walsh, P., 2002. Modeling of grabens extending above evaporites in Canyonlands Natioal Park, Utah. Journal of Structural Geology 24, 247–275.

Vendeville, B.C., 1987. Champ de failles et tectonique en extension: modélisation experimentale. Ph.D. thesis, Université de Rennes, Rennes.

Vendeville, B.C., Jackson, M.P.A., 1992. The rise of diapirs during thin-skinned extension. Marine and Petroleum Geology 9, 331–353.

Vendeville, B.C., Cobbold, P.R., Davy, P., Brun, J.P., Choukroune, P., 1987. Physical models of extensional tectonics at various scales. In: Cowards, M.P., Dewey, J.F., Handcock, P.L. (Eds.), Continental Extensional Tectonics. Geological Society Special Publication 28, pp. 95–107.

Werijermars, R., Jackson, M.P.A., Vendeville, B.C., 1993. Rheological and tectonic modeling of salt provinces. Tectonophysics 217, 143–174.

Wernicke, B., 1981. Low-angle normal faults in the Basin and Range Province: nappe tectonics in an extending orogen. Nature 291, 645–648.

Wernicke, B., 1985. Uniform-sense normal simple shear of the continental lithosphere. Canadian Journal of Earth Sciences 22, 108–125.

Withjack, M.O., Callaway, S., 2000. Active normal faulting beneath a salt layer: experimental study of deformation patterns in the cover sequence. American Association Petroleum Geologists Bulletin 84, 627–651.